Ore Geology Reviews 86 (2017) 254–270

Contents lists available at ScienceDirect

Ore Geology Reviews

journal homepage: www.elsevier.com/locate/oregeo

Geology, fluid inclusion and stable isotope study of the Yueyang Ag-Au-Cu deposit, Zijinshan orefield, Fujian Province, China

Jun Zhong [a,b], Yan-Jing Chen [b,*], Jin-Ping Qi [c], Jing Chen [b], Mao-Chang Dai [c], Jing Li [c]

[a] Beijing Research Institute of Uranium Geology, Beijing 100029, China
[b] Key Laboratory of Orogen and Crust Evolution, Peking University, Beijing 100871, China
[c] Zijin Mining Group Co. Ltd, Shanghang 364200, Fujian, China

ARTICLE INFO

Article history:
Received 26 June 2016
Received in revised form 19 February 2017
Accepted 22 February 2017
Available online 27 February 2017

Keywords:
Fluid inclusion
Stable isotope geochemistry
Yueyang Ag-Au-Cu deposit
Low-sulfidation
Zijinshan orefield
Fujian Province, China

ABSTRACT

The large Yueyang Ag-Au-Cu deposit is commonly regarded as a low-sulfidation epithermal deposit in the Zijinshan orefield, Fujian Province, southeastern China. The Ag-Ag-Cu orebodies hosted in the Zijinshan granitic batholith are mainly stratoid and lens in shape, and controlled by a series of NW-trending listric faults with shallow dip angles. Four mineralization stages are recognized on the basis of mineral assemblage, ore fabrics, and crosscutting relationships of the ore veins, namely: pre-ore (pyrite + sericite + quartz ± chlorite), main Cu (chalcopyrite + pyrite + sericite + quartz ± bornite), main Ag-Au (Ag and Au minerals + pyrite + quartz + adularia ± calcite ± apatite ± chalcopyrite ± galena ± sphalerite) and post-ore (quartz ± chalcedony ± calcite) stages. Fluid inclusions (FIs) in the deposit include aqueous liquid-rich (WL-), aqueous vapor-rich (WV-), and minor carbonic (C-) and daughter mineral-bearing (S-) type ones. WL-subtype is the main inclusion type in the Yueyang deposit, accounting for more than 90% in proportion in each stage. Minor WV-subtype inclusions occur in both the main Cu and Ag stages, while the C-type and S-type ones are only observed in the main Cu stage. Fluid inclusion and H-O isotope study indicated that the ore-forming fluid of the main Cu stage is primarily magmatic vapor, which further underwent fluid boiling and mixing with meteoric water, while the ore-forming fluid of the main Ag stage is meteoric water-dominated, and the precipitation of silver and gold was mainly resulted from fluid boiling and the precipitation of other sulfides. On the basis of the aforementioned geological, fluid inclusion and stable isotope studies, we proposed a two-stage model for the Yueyang deposit, including a magmatic vapor-related porphyry type Cu mineralization and meteoric water-related low-sulfidation epithermal Ag-Au-Cu mineralization, although the porphyry Cu mineralization is very limited in scale. The mineralization and exhumation depths of the Yueyang deposit are estimated to be 448 527 m and 18 97 m, respectively. By comparison with the exhumation depths of other deposits in the Zijinshan orefield, it is suggested that more epithermal deposits could be found in the southwest of the orefield due to less uplift and exhumation therein.

1. Introduction

Since the late 1970s, the understanding of epithermal deposits was largely improved when exploration interest rose due to the increasing value of gold and silver, and a dozen classification schemes have been proposed, with the high-sulfidation and low-sulfidation subtypes (Hedenquist, 1987) most commonly used. Most of the high-sulfidation deposits are mined for Au and Cu as exemplified by Lepanto, Philippine (Hedenquist et al., 1998; Chang et al., 2011), Chinkuashih, Taiwan (Wang et al., 1999; Wang, 2010), Summitville, USA (Stoffregen, 1987), Pascua, Chile (Chouinard et al., 2005), while the low-sulfidation deposits usually lack large-scale Cu mineralization but favor Au, Ag, as well as base metals like Pb, Zn, e.g., Hishikari, Japan (Faure et al., 2002), Hauraki goldfields, New Zealand (Brathwaite and Faure, 2002; Simmons et al., 2005), Apacheta, Peru (André-Mayer et al., 2002), and those in North Xinjiang (Zhai et al., 2009; Chen et al., 2012) and West USA (John, 2001; John et al., 2003). Hydrothermal processes linked to Au-Ag mineralization and alteration are well understood in these deposits, with fluid boiling, mixing, conductive cooling and wall rock interaction as the effective ore-precipitation mechanisms (Hedenquist and Henley, 1985; Canet et al., 2011; Drummond and Ohmoto, 1985; Hedenquist et al., 1998). However, the genetic relationship between magmatic water and epithermal deposits,

* Corresponding author at: Department of Geology, Peking University, Beijing 100871, China.
E-mail address: yjchen@pku.edu.cn (Y.-J. Chen).

http://dx.doi.org/10.1016/j.oregeorev.2017.02.023
0169-1368/

especially low-sulfidation ones, remains the subject of continued debate (Hedenquist and Lowenstern, 1994; John et al., 2003; Simmons et al., 2005).

The Yueyang Ag-Au-Cu deposit, also known as the Bitian deposit in many Chinese literatures (Chen et al., 1997a,b; Zhang et al., 2003a; Liu and Hua, 2005), is located about 3 km southwest to the Zijinshan Cu-Au deposit (Fig. 1), and recognized as a typical low-sulfidation epithermal deposit since its discovery in the late 1980s (Lin, 2006; Liu and Hua, 2005; Chen et al., 1997a,b; So et al., 1998). The large Ag-Au-Cu deposit can be divided into the east and west sections (Fig. 1), and holds total reserves of 1330 t Ag at average grade of 137.6 g/t, 8.2 t Au at 0.7 g/t and 0.04 Mt Cu at 0.9% (Zhang, 2013). The Ag-Au-Cu orebodies are stratiform or lens in shape and controlled by a series of NW-trending listric faults. They are mainly hosted in the Jurassic Zijinshan granitic batholith between the Neoproterozoic basement and overlying Cretaceous volcanic rocks (Fig. 3; Lin, 2006; Zhang et al., 2003a, b). Adularia grains intergrown with Au-Ag minerals yielded ^{40}Ar ^{39}Ar ages of 91.5 ± 0.4 Ma (Liu and Hua, 2005) and 94.7 ± 2.3 Ma (Zhang et al., 2003a). Besides, Zhang et al. (2003b) reported two sericite ^{40}Ar ^{39}Ar ages of 102.9 ± 1.9 Ma and 102.5 ± 1.5 Ma from phyllic alteration rocks in the Yueyang and Wuziqilong deposits (Zhang et al., 2003b), respectively, which are coeval to the alunite ^{40}Ar ^{39}Ar age (~103 Ma) in the Zijinshan

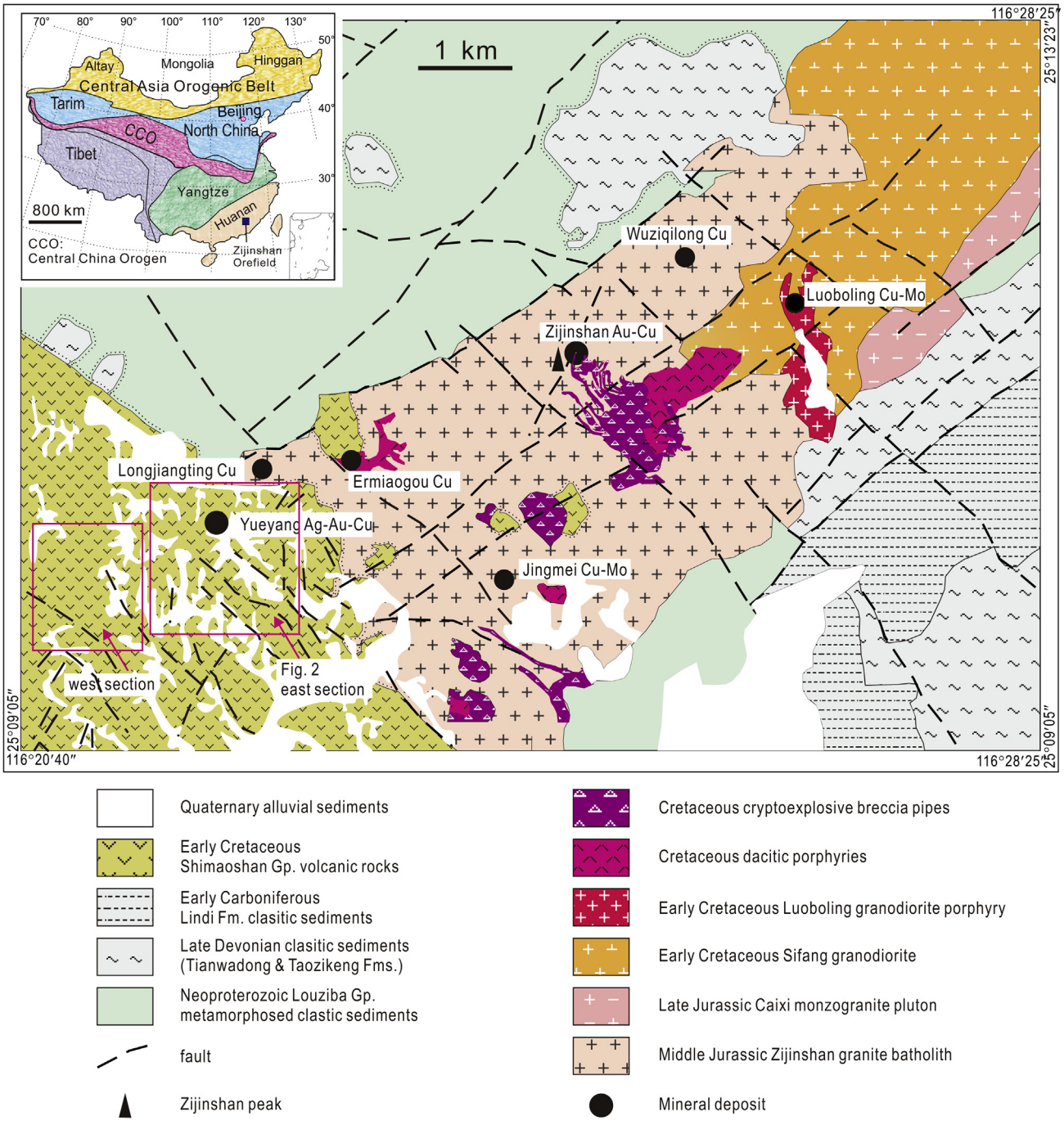

Fig. 1. Geological map of the Zijinshan Orefield (modified after Zhong et al., 2014).

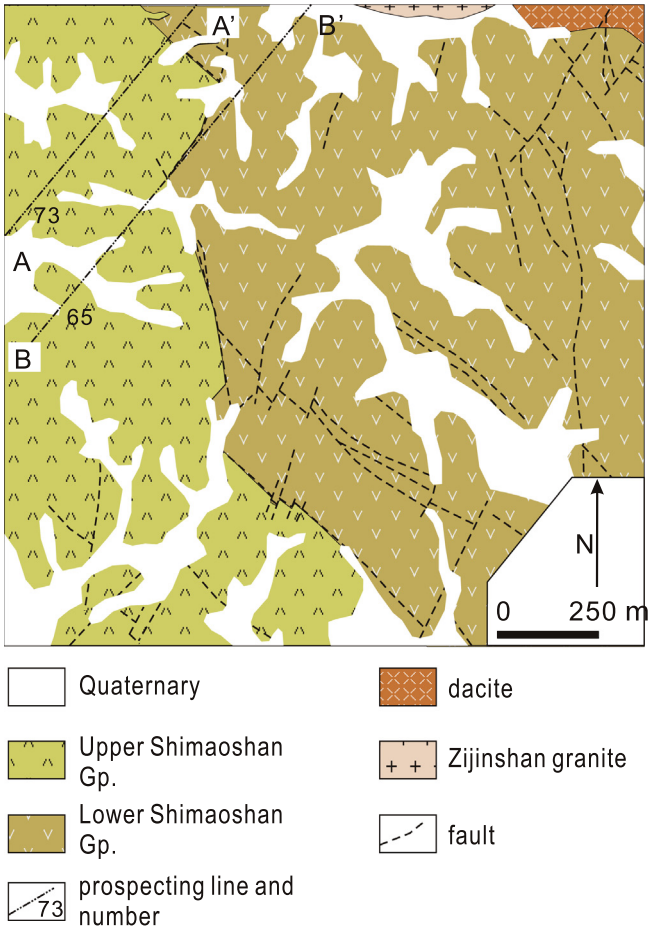

Fig. 2. Geological map of the east section in the Yueyang Ag-Au-Cu deposit (modified after unpublished data from Zijin Mining Group Co., Ltd, 2008).

deposit (unpublished data), but slightly later than the molybdenite Re Os isochron age (104.6 ± 1.0 Ma, Zhong et al., 2014) in the Luoboling porphyry Cu-Mo deposit.

In general, the geological and geochronologic studies of the Yueyang deposit indicated that it is a low-sulfidation epithermal deposit formed during ~95 91 Ma. However, the mineral paragenesis, ore-precipitation mechanism and ore-forming fluid evolution history of the Yueyang deposit are still poorly constrained. In this contribution, detailed electron microprobe, fluid inclusion, Laser Raman spectroscopic and stable isotopic studies are carried out, to determine the characteristics and evolution process of the ore-forming fluids, as well as the possible ore transportation and deposition mechanism of ore minerals.

2. Regional and deposit geology

The comprehensive descriptions of regional geology of the Zijinshan orefield are by So et al. (1998), Zhang et al., (2003b), and Zhong et al. (2014, 2017a,b). The regional geology of the Zijinshan district is shown in Fig. 1. The Neoproterozoic Louziba Group low-grade metamorphic rocks and Late Paleozoic lithologic sequences were folded into the NE-trending Xuanhe anticlinorium, which was subsequently intruded by the Early Yanshanian (Middle to Late Jurassic) Zijinshan granitic batholith and overlain by the Late Yanshanian (Early Cretaceous) volcanic rocks of the Shimaoshan Group. The volcanic rocks extensively crop out in the Yueyang volcanic basin and locally exposed in the Zijinshan mining district in the northeast of the orefield due to rapid uplift and exhumation herein (Fig. 1). Detailed geochronologic studies revealed two distinct magmatic events in the Zijinshan orefield: the Early Yanshanian granitoids and Late Yanshanian granodioritic volcanic and intrusive rocks (Huang et al., 2013; Jiang et al., 2013; Zhao et al., 2008; Mao et al., 2002; Zhang et al., 2001; Wu et al., 2013). Sporadic W and Sn mineralization was discovered in the Early Yanshanian granites (Liu et al., 2016), but of no important economic significance. Cu, Au, Mo and Ag mineralization in the orefield are regarded to be genetically associated with the Late Yanshanian granodioritic magmatic rocks as they share intimate spatial and temporal relationships (So et al., 1998; Zhang et al., 2003b; Zhong et al., 2014, 2017a,b). Faults and fractures in the orefield are mainly NE- and NW-trending, dividing the district into several rhombic blocks hosting the Cu-Au-Mo deposits (Fig. 1).

The Yueyang Ag-Au-Cu deposit is located at the northeastern margin of the Yueyang volcanic basin, nearly 3 km southwest to the Zijinshan Cu-Au mining district. It is further divided into the east and west mining sections (Fig. 1), which are exploited by different companies but share the exact same geological characteristics. The east mining section hosts nearly 2/3 of the total metal reserves of the Yueyang Ag-Au-Cu deposit and all samples in this study were collected herein. As revealed by drilling, the Neoproterozoic Louziba Group is the oldest lithologic unit in the Yueyang Ag-Au-Cu deposit (Fig. 3), consisting of two-mica or muscovite schist (Fig. 4f), phyllite, and low-grade metamorphic fine-grained sandstone, siltstone. The pre-Mesozoic rocks are intruded by the Jurassic Zijinshan granitic batholith, which is composed of the Jingmei coarse-grained cataclastic granite (Fig. 4c), the Wulongzi (or Wulongsi) medium- to fine-grained granite (Fig. 4d) and the Jinlongqiao fine-grained muscovite granite (Fig. 4e), with LA-ICP-MS zircon U–Pb ages of 165 ± 1, 164 ± 1, and 157 ± 1 Ma, respectively (Jiang et al., 2013). The volcanic rocks of the Shimaoshan Group unconformably overlying the granite batholith can be divided into two parts on the basis of lithologic variation. The upper part volcanic rocks, with local U mineralization, are composed of rhyolite (Fig. 4b), rhyolitic volcanic breccia, tuff, and tuffaceous sandstone, while the lower part ones are mainly hornblende and biotite trachyandesite (Fig. 4a), with minor andesite, dacite, sandstone and conglomerate. These rocks (volcanic, granitic and metamorphic rocks) consist of a "sandwich-like" lithologic distribution in the Yueyang deposit, with Au-Ag-Cu orebodies intercalated in the middle granitic rocks (Fig. 3). The overlying Shimaoshan Group volcanic rocks were locally covered by Quaternary sediments (Fig. 2).

Ag-Au-Cu orebodies in the Yueyang deposit are concealed and controlled by a series of listric normal faults or fractures. They are mostly hosted in the granitic batholith (Fig. 3), especially the Wulongzi medium- to fine-grained granite, but locally in the Lower Shimaoshan Group trachyandesite (Liu and Hua, 2005; Chen et al., 1997a,b). The ore veins are stratoid or lens in shape striking 290°–320° and dipping to the NE or SW with shallow angles (<20°) (Fig. 3a, b). Major orebodies of the east section (No. 1, 2, 3 orebodies, Fig. 3) account for 87.1% silver, 83.0% gold and 66.5% copper of the total metal reserves of the east section, showing a flattened V-shaped appearance in cross section profiles (e.g., Fig. 3a). The average ore grade of copper increased, but silver and gold grade decreased towards shallower parts.

3. Sample selection and analytical techniques

More than seventy samples of ores and host rocks were collected from No. 1 and No. 2 orebodies in the adits at elevations of −160 m, −130 m, and −100 m above sea level (asl.). Fifty double-polished thin sections (0.03 mm thick) were made for petrologic study, using both optical and electron microprobes. Forty-seven double-polished thin sections (~0.3 mm thick) were made for fluid inclusion study, and thirteen of them (listed in

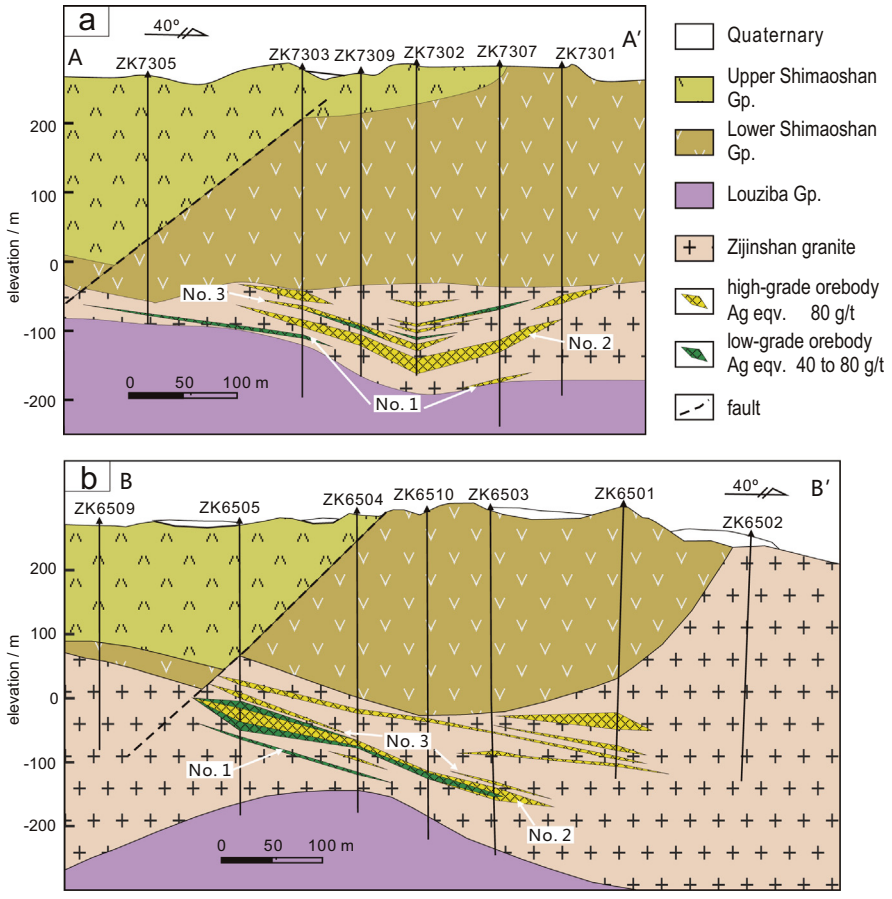

Fig. 3. Geological profiles along prospecting lines No. 73 (a) and No. 65 (b) of the Yueyang Ag-Au-Cu deposit (modified after unpublished data from Zijin Mining Group Co., Ltd, 2008).

Table 1) were chosen for microthermometric and Laser Raman spectroscopic analyses. Eleven samples (listed in Table 4) were selected for stable isotopic analysis.

The electron microprobe microanalyses of minerals were carried out on a JEOL JXA-8100 electron microprobe in the Key Laboratory of Orogen and Crust Evolution, Peking University. Operating conditions were 20 kV accelerating voltage, 10 nA beam current with 10 s measurement time and 1 μm spot size. Natural and synthetic minerals by the American SPI were used as standards. The ZAF method was used for data reduction for sulfides.

Microthermometric measurements were carried out using a Linkam THMSG 600 freezing-heating stage at the Institute of Geology and Geophysics, Chinese Academy of Sciences (IGGCAS), Beijing. Temperatures were calibrated using synthetic fluid inclusions provided by FLUID INC, USA. The precisions for the measured temperatures are estimated better than ±0.5, ±0.2, and ±2 °C at the temperature ranges of −120 to −70 °C, −70 to 100 °C, and 100 to 500 °C, respectively. During freezing/heating runs, the freezing/heating rates were constrained at 1–10 °C/min, and reduced to 0.5–1 °C/min near phase transformation points. Salinities (reported in wt% NaCl eqv.) and densities (g/cm^3) of the aqueous (NaCl-H_2O) and carbonic (CO_2-H_2O) inclusions were calculated based on final ice points (Bodnar, 1993) and the final temperatures of CO_2-clathrate (Collins, 1979) using the program Flincor (Brown, 1989).

Laser Raman spectroscopic (LRS) analyses were performed at the Key Laboratory of Orogen and Crust Evolution, Peking University, Beijing. The laser source was an argon laser with wave length of 514.5 nm and a source power of 1000 mW. Integration time was 10 s, with ten accumulations for each spectral line. The spectral resolution is ±2 cm^{-1} with a beam size of 2 μm.

Quartz grains for hydrogen and oxygen analyses were extracted from crushed and washed rock samples, and purified by hand picking under binocular microscope. Eleven quartz samples (listed in Table 4) from different stages were analyzed in the Stable Isotope Laboratory of Mineral Resources Institute, Chinese Academy of Geological Sciences, using the Finnigan MAT253 mass spectrometer. Oxygen was liberated from quartz by reaction with BrF_5 (Clayton and Mayeda, 1963) and converted to CO_2 on a platinum-coated carbon rod for oxygen isotope analysis. The water of the fluid inclusions in quartz was released by heating the samples to above 500 °C by means of an induction furnace, and then reacted with chromium powder at 800 °C to generate hydrogen for isotope analysis (Wan et al., 2005). The results were reported in per mil relative to V-SMOW standards, with precisions of ±2‰ for δD and ±0.2‰ for $\delta^{18}O$. The $\delta^{18}O$ values of ore-forming fluids from quartz were calculated using the equation $1000\ln\alpha_{quartz\text{-}H2O} = 3.38 \times 10^6\, T^{-2} - 3.4$ (Clayton et al., 1972).

4. Mineral paragenesis and mineralization stages

On the basis of mineral assemblages, ore fabrics and crosscutting relationships, four mineralization stages are identified, namely, pre-ore, main Cu, main Ag (or Ag-bearing polymetallic) and post-ore (or late) stages (Fig. 5).

4.1. Pre-ore stage

Pre-ore mineral assemblages, pervasively observed in the mining district, are composed of pyrite, sericite, and minor

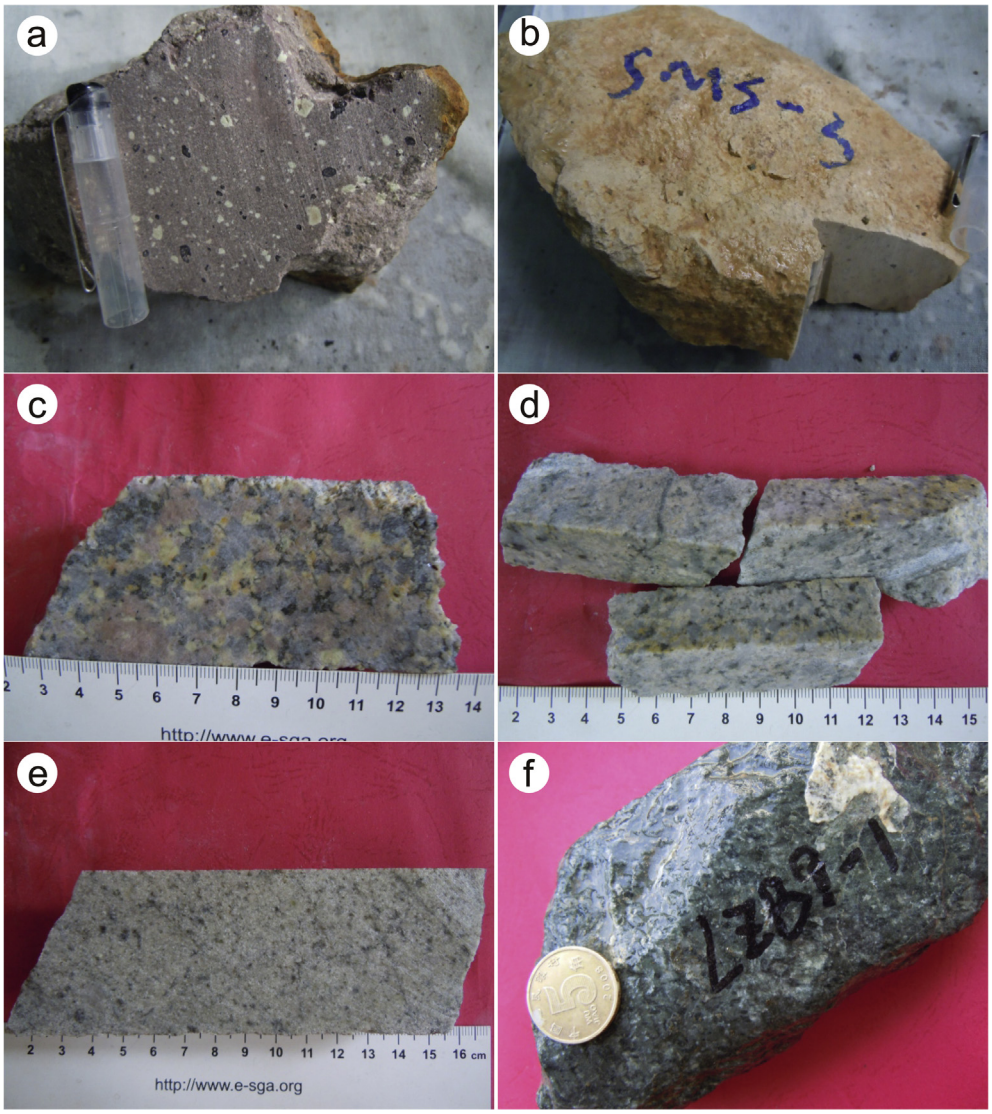

Fig. 4. Photos showing the petrology of the main rocks in the Yueyang deposit. (a) Trachyandesite of the lower Shimaoshan Group; (b) rhyolite of the upper Shimaoshan Group; (c) Jingmei coarse-grained cataclastic granite; (d) Wulongzi (or Wulongsi) medium- to fine-grained granite; (e) Jinlongqiao fine-grained muscovite granite; (f) mica schist of the Lowziba Group.

Table 1
Geological characteristics of selected samples from the Yueyang Ag-Au-Cu deposit for fluid inclusion study and Laser Raman spectroscopy.

Sample No.	Mineralization stage	Mineralization style	Major minerals	Host mineral	Analyzing method*
Y-04a	Main Cu stage	Disseminated, veinlets	Py, Ccp, Qtz, Srt	Qtz	FI
Y-11	Main Cu stage	Stockworks	Ccp, Py, Srt, Qtz	Qtz	FI, LRS
Y-14	Main Cu stage	Massive	Py, Ccp, Gn, Srt, Qtz	Qtz	FI
130-2-M	Main Cu stage	Breccia, massive	Ccp, Py, Gn, Sp, Qtz	Qtz	FI, LRS
Y-03	Main Ag stage	Vein	Ccp, Qtz	Qtz	FI
Y-02a	Main Ag stage	Vein	Slv, El, Kut, Gn, Sp, Py, Qtz, Adl, Cc	Qtz	FI
Y-07	Main Ag stage	Massive	Gn, Sp, Py, Slv, Qtz, Ill	Qtz	FI
Y-06	Main Ag stage	Vein	Sp, Ccp, Py, Slv, Qtz, Adl	Qtz	FI, LRS
160-12	Main Ag stage	Massive	Gn, Sp, Qtz	Qtz	FI
$160B_1$	Main Ag stage	Veinlet	Sp, Qtz	Sp	FI, LRS
$130\text{-}B_2\text{-L}$	Late stage	Vein	Qtz, Cc	Qtz	FI, LRS
Y-05-L	Late stage	Vein	Qtz	Qtz	FI
130-2-L	Late stage	Vein	Qtz, Cc	Qtz	FI

Abbreviations: Adl, adularia; Arn, argentite; Cc, calcite; Ccp, chalcopyrite; El, electrum; Gn, galena; Ill, illite; Kut, kustelite; Py, pyrite; Qtz, quartz; Sp, sphalerite; Slv, native silver; Srt, sericite.

* FI: fluid inclusion study; LRS: Laser Raman spectroscopy.

coarse-grained quartz and chlorite. Sericite aggregates with the subhedral pyrite grains replaced feldspar along grain boundaries and microfractures (Fig. 7a, b) in the slightly altered granite rocks. In the intensively altered or mineralized Cu and Ag ores, either sericite- or pyrite-dominated clusters are surrounded by later-stage fine-grained quartz. Pyrite grains from this stage are usually

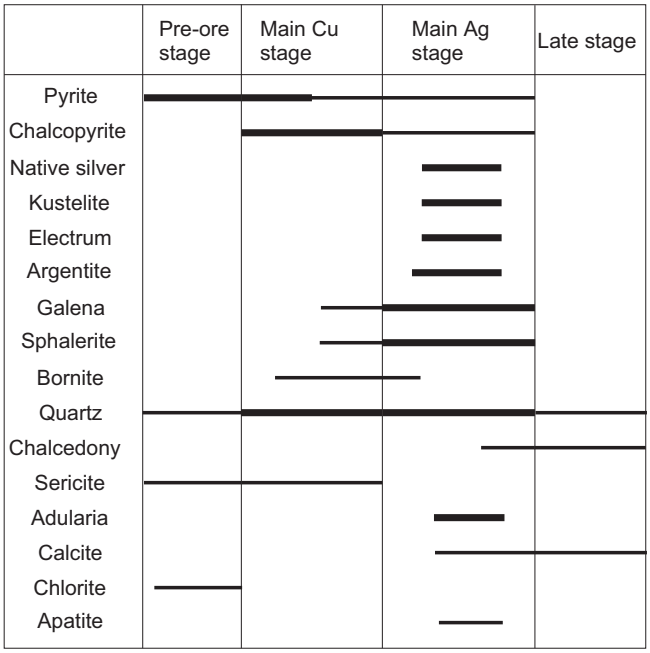

Fig. 5. Mineral paragenesis of the Yueyang Ag-Au-Cu deposit.

replaced by chalcopyrite (Fig. 7c), galena and sphalerite (Fig. 7i). Chemical compositions of the pyrites are relatively stable, with minor amount of Ag (<0.05 wt%) and variable contents of Cu (0.21 1.26 wt%) (Table 2).

The pyrite-sericite assemblages are not only observed in the Yueyang Ag-Au-Cu deposit, but also in the Zijinshan Cu-Au (in preparation), Wuziqilong Cu (Chen et al., 2011) and Longjiangting Cu (Chen, 2013; Chen et al., 2015) deposits, indicating a pre-ore hydrothermal process all over the orefield.

4.2. Main Cu (Ccp-Py ± Bn) stage

The pre-ore pyrite- and sericite-bearing granite rocks were fractured or brecciated in this stage and crosscut by chalcopyrite-dominated veins or stockworks (Fig. 6a, b). Fine- to medium-grained anhedral smoky quartz is the main gangue mineral, accompanied by minor sericite aggregates. They are intergrown with chalcopyrite grains, and subsequently overprinted or surrounded by fine-grained quartz grains (Fig. 7d, e). Chalcopyrite in this stage sometimes coexisted with fine- to medium-grained (less than several hundred micrometers) galena and sphalerite, replacing pyrite of the pre-ore stage (Fig. 7c, i). They contain minor Ag (<0.07 wt%), Au (<0.14 wt%) and As (<0.04 wt%) contents (Table 2). Sphalerite is dark brown in color and contains 0.79–1.41 wt% Fe and 0.33–0.38 wt% Cd (Table 2).

Another quartz-dominated vein-type Cu mineralization, mainly comprised of euhedral chalcopyrite, quartz, pyrite grains (Figs. 6c and 7f), and sometimes intergrown with bornite (Fig. 7g, h), was discovered but of less economic importance in the Yueyang deposit. Unlike those in the brecciated or stockwork Cu ores, quartz grains in the veins show better morphology and transparence (Figs. 6c and 7f). From margin to center of the veins, the mineral grains varied from several micrometers white quartz to centimeters of light purple amethyst (Fig. 6c). Typical open space filling structures, such as geodes and quartz druses, indicated that these veins were formed in a stable environment at relatively low temperatures.

4.3. Main Ag (Ag-bearing polymetallic) stage

Ag- and Au-bearing ore minerals mainly occur in several centimeter-wide veins (Fig. 6e, f), or massive smoky ores, which are usually crosscut by late-stage barren white quartz veins (Fig. 6g). It is observed that the brecciated Cu ores are cut by the silver-bearing veins (Fig. 6a), and the chalcopyrite-pyrite-quartz veins are usually cut by galena-sphalerite-quartz veins (Fig. 6d). Moreover, it is common that the chalcopyrite-sericite (or illite)-quartz assemblage clusters of the main Cu stage are surrounded by the Ag or Au mineralization-related silicic alteration in the Ag or Au ores (Figs. 7d, e and 8g), also suggesting that the main Ag stage postdated the main Cu stage. Nevertheless, some chalcopyrite grains share common boundaries with native silver (Fig. 8c), native silver-bearing galena (Fig. 8b), argentite (Fig. 8e) or sphalerite crystals, signifying that the Cu mineralization had a prolonged evolution history and also took place during the main Ag stage.

Ore minerals of this stage are mainly native silver, gold, argentite, electrum, kustelite, chalcopyrite, pyrite, galena and sphalerite, while the major gangue minerals are quartz, adularia, calcite and apatite. Ore minerals are often located at the margin of hydrothermal veins with some fine-grained illite, quartz, adularia (Fig. 8h), calcite (Fig. 8i) and apatite, but diminished in the center of the veins, where euhedral coarse-grained quartz and minor calcite crystals are the predominant minerals in comb structure (Fig. 6e, f). Geode filling of sulfides is observed at the margin of the ore veins as shown in Fig. 6e. The Ag or Au minerals, such as native silver, electrum, kustelite, argentite, are usually fine-grained (1–10 μm) and occur as inclusions in pyrite (Fig. 8a) and galena (Fig. 8b, d), and less commonly in sphalerite and quartz. Coarse-grained (several hundred micrometers) native silver or argentite grains are intergrown with pyrite, galena and chalcopyrite (Fig. 8c, e). Chalcopyrite in this stage, especially those accompanying with the Ag minerals, often contains higher Ag (up to 10.57 wt%) but lower Fe contents (as low as 26.01 wt%) than those in the main Cu stage (Table 2). More detailed electron probe microanalyses (Chen et al., 1997a) revealed a distinct negative correlation between both Fe, Cu and Ag, indicating that Ag exist in the crystal lattice as isomorphism of both the Fe and Cu. Galena, pyrite and sphalerite in this stage have relatively stable chemical compositions and low Ag contents. Sphalerite grains, from several hundred micrometers to several centimeters in size, are red brown or light yellow in color and contain low Fe contents (<0.64 wt%). Much of the sphalerite grains are always dusted by minute chalcopyrite inclusions (Fig. 9g, h). Crustiform pyrite grains are locally found and surrounded by later co-depositional assemblage of pyrite and chalcopyrite in this stage.

Most of the adularia crystals, in the form of small rhombic, euhedral crystals (<300 μm), are sparsely distributed in the Ag mineral-bearing quartz veins, and fill in the cavities between coarse-grained quartz grains, or as inclusions in them (Fig. 8h). Minor adularia plates are also found in the altered granite rocks hosting the Ag-bearing veins, replacing sericite plates as aggregates. Calcite and native silver fill in the geodes as vug linings (Fig. 8i). Platy quartz is observed in several samples, which is demonstrated as the result of dissolutions of early-formed platy calcite during cooling, and subsequent silica filling (Simon et al., 1999; Zhai et al., 2009).

In addition to the Ag- or Au-bearing ores, another type of sphalerite-galena-dominated massive ores (Fig. 6h and 8f) was discovered in Yueyang deposit and of less economic importance, mainly comprising of sphalerite, galena and quartz, without Ag- or Au-minerals.

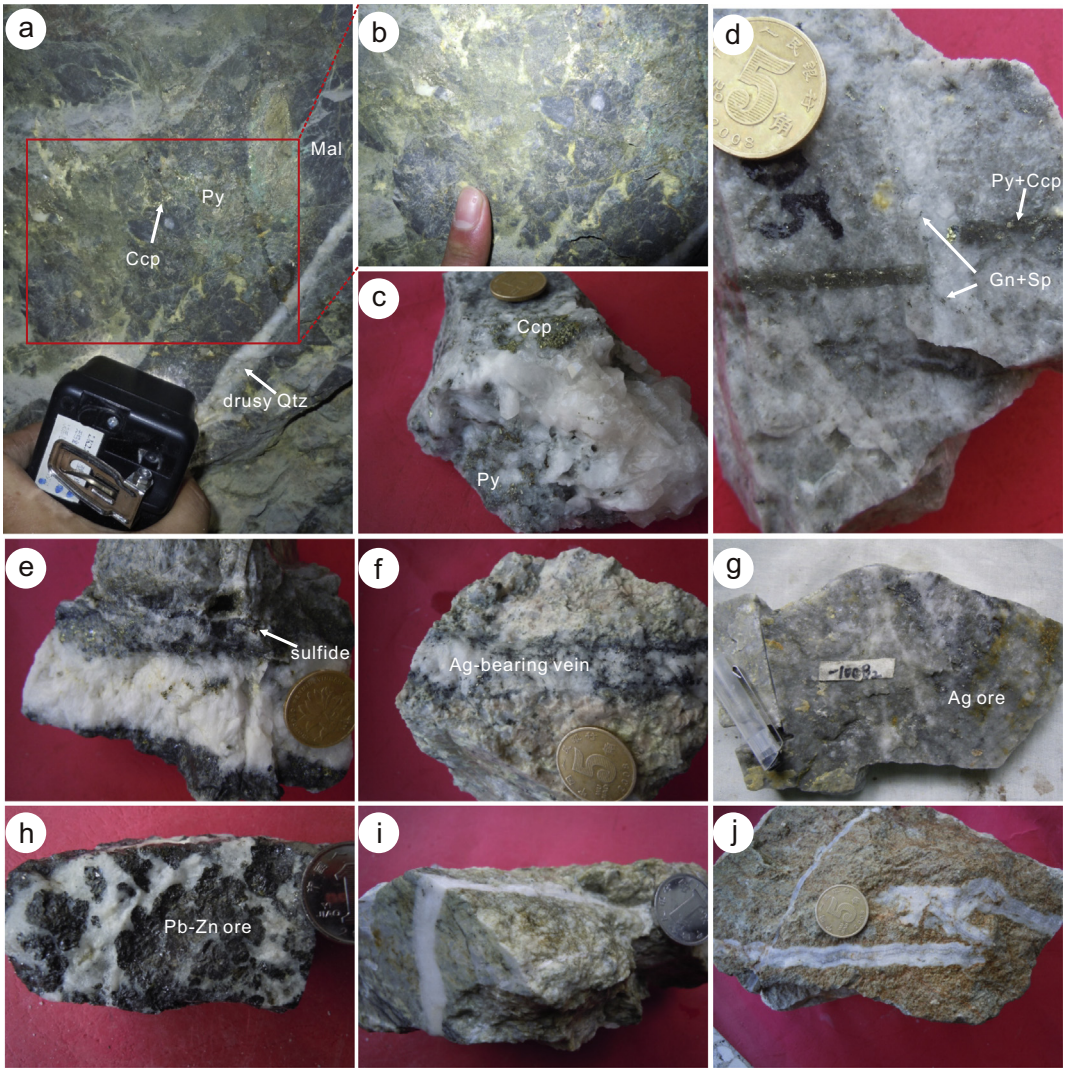

Fig. 6. Photographs showing ore fabrics of each mineralization stage in the Yueyang Ag-Au-Cu deposit. (a) Pre-ore sericite-pyrite assemblage was brecciated and cemented by chalcopyrite and pyrite, and malachite was formed by later fluid-rock interaction. Note that the brecciated Cu ores were cut by native silver-bearing quartz veins. (b) Box area in Fig. 6a, showing the same ore textures. (c) Later chalcopyrite-quartz vein, with chalcopyrite and minor pyrite in the margin but euhedral and coarse quartz (and amethyst) grains in the center of the vein. (d) Minor galena and sphalerite-bearing quartz vein cut the pyrite-chalcopyrite-quartz vein. (e) Ag-bearing polymetallic ore veins (~3 cm in width), showing comb quartz, miarolitic and drusy structures. (f) Native silver and argentite-bearing quartz vein in the coarse-grained granite. (g) Intensively silicified massive dusty Ag-bearing ores was cut by late-stage white quartz stockworks. (h) Massive Pb-Zn ore, predominantly composed of galena, sphalerite and quartz. (i) Late-stage quartz-calcite vein in medium- to coarse-grained granite, cutting sulfide stockworks. (j) Late-stage quartz-chalcedony-amethyst vein in volcanic rock, showing colloform structures. Abbreviations: Ccp, chalcopyrite; Py, pyrite; Mal, malachite; Qtz, quartz; Gn, galena; Sp, sphalerite.

4.4. Post-ore stage

Barren white quartz veins cut all the ores (Fig. 6d, g) and marked the termination of fluid evolution in the Yueyang deposit. Much of the veins are comprised of fine-grained quartz and chalcedony (Fig. 6d, g, i). Comb structure and geodal filling of drusy quartz, amethyst and minor calcite, as well as colloform-crustiform textures (Fig. 6j), are common in these veins.

5. Fluid inclusion study

Thirteen samples, either vein-type or massive ores of every mineralization stage, were selected for fluid inclusion petrographic and microthermometric studies (Table 1). Abundant fluid inclusions (FIs) in quartz grains in different ore mineral-bearing veins or massive ores were analyzed. The euhedral to subhedral quartz crystals are generally millimeters to centimeters in size, and display no re-crystallization features such as subgrain boundaries or undolose extinction. We select those quartz crystals adjacent to or surrounded by sulfides (Fig. 9a), which are interpreted to precipitate nearly simultaneously (Wilkinson, 2001). Therefore, primary and pseudosecondary fluid inclusions in quartz grains, identified using the criteria of Roedder (1984), are interpreted to have trapped ore fluid that transported silver, gold and copper during the formation of the ores. In addition to quartz crystals, several sphalerite grains with low Fe content and relatively high transparence are also chosen for fluid inclusion studies (Table 1; Fig. 9g, h).

5.1. Fluid inclusion types and assemblages

Three types of fluid inclusions were identified based on their phases at room temperatures (21 °C), phase transitions during heating and cooling (−100 to 400 °C), and laser Raman spectroscopy (Chen et al., 2007). They are predominately consisted of

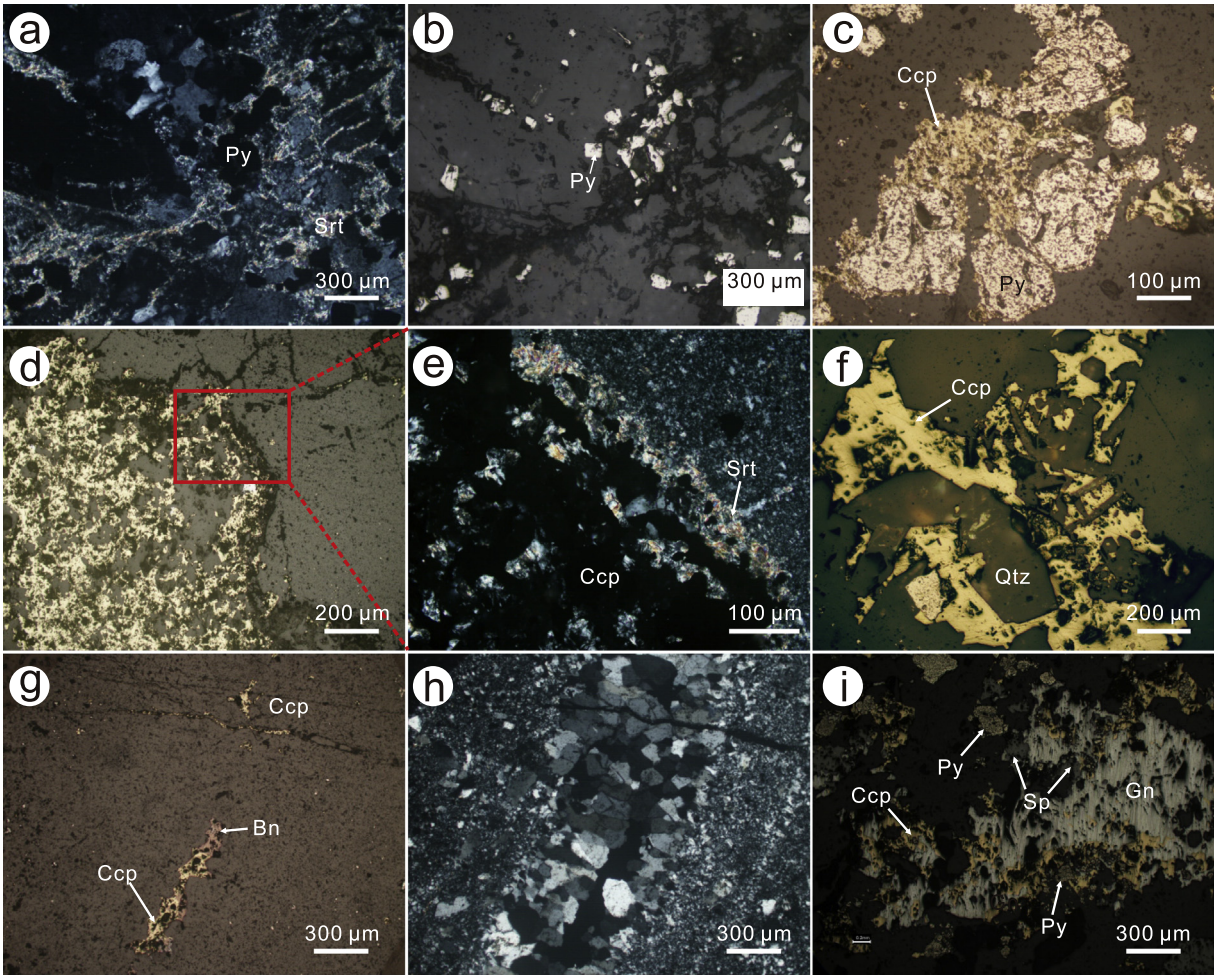

Fig. 7. Photomicrographs showing mineral assemblages and textures of the pre-ore and main Cu mineralization stages in the Yueyang Ag-Au-Cu deposit. Granitic rock is altered and crosscutted by sericite and pyrite stockworks of the pre-ore stage, crossed polars in (a) and reflected light in (b). (c) Chalcopyrite replaced pyrite in the main Cu stage. (d) Chalcopyrite-sericite-quartz cluster is overprinted and surrounded by the later fine-grained quartz grains (reflected light). (e) Chalcopyrite intergrown with sericite in the main Cu stage, the area is box in d (crossed polars). (f) Chalcopyrite intergrown with euhedral quartz grains in the main Ag stage. (g) Chalcopyrite-bornite quartz vein with comb texture is cut by later chalcopyrite stringer (reflected light). (h) Same area as Fig. 7g (crossed polars). (i) Pyrite grains, replaced by galena, sphalerite and chalcopyrite, occur as residual islands. Abbreviations: Bn, bornite; Ccp, chalcopyrite; Py, pyrite; Gn, galena; Sp, sphalerite; Qtz, quartz; Srt, sericite.

aqueous inclusions, with few carbonic and solid-bearing ones (Fig. 9).

The aqueous (W) type FIs are two-phase (liquid and vapor water) NaCl-H_2O systems (Fig. 9b, c, f, g, h), which are further divided into liquid-rich (WL) and vapor-rich (WV) subtypes according to vapor/(vapor + liquid) [V/(V + L)] ratio and homogenization mode. WL-subtype FIs, commonly with 5–20 vol% vapor phase, are the predominant type (>90% in proportion of each stage) in the Yueyang deposit and mostly homogenize into a liquid phase. These FIs are usually round, ellipsoid, negative crystal in shape and 5–20 μm in size (Fig. 9b, c, g, h), with several exceptions up to 30 μm. WV-subtype FIs are less common and only identified in two samples. These FIs, with V/(V + L) ratio >60% and maximum dimensions ranging from 5 to 15 μm, often display round and negative crystal shapes (Fig. 9f), and all homogenized into vapor phase on heating run.

The carbonic (C) type FIs are two-phase (vapor CO_2 + liquid H_2O) CO_2-H_2O system, with CO_2 phase accounting for 60–90% in volume. These FIs, isolated or clusters in occurrence, are ellipsoid and negative crystal in shape and 10–20 μm in size (Fig. 9d, f). These FIs were only observed in one sample (Y-11) and only three of those analyzed for further microthermometric measurements came out with convincible results as these FIs share ambiguous vapor-liquid boundaries.

The solid-bearing (S) type FIs refer to the daughter mineral-bearing FIs, consisting of one or more daughter minerals. They are ellipsoid, irregular and negative crystals in shape and 5–25 μm in size. Daughter minerals contain transparent halite and sylvite, while opaque minerals include red hematite and unidentified dark ones (Fig. 9e), which are too small to be revealed by Raman spectroscopic analyses. Only two S-type inclusions were analyzed in the sample Y-11 (Table 3).

Besides the forementioned FIs, another type of pure aqueous (PW) FIs were also identified, mostly coexisted with WL-subtype FIs of low V/(V + L) ratios (<10 vol%) in fractures or fissures cutting crystal boundaries. These FIs were clearly secondary in origin and cannot represent the ore-forming fluids.

Primary inclusions belonging to one intragranular trail or clusters were regarded as a fluid inclusion assemblage (FIA; Goldstein and Reynolds, 1994; Goldstein, 2001). In the Yueyang deposit, three types of FIAs are recognized: (1) consisting only of WL-subtype inclusions; (2) consisting of WL + WV ± C ± S-type inclusions; (3) consisting of WL- and PW-type FIs. FIA 1 is commonly seen in both the main Cu and Ag stages. The primary WL-

Table 2
Electron probe microanalysis of major ore minerals in the Yueyang deposit (wt%).

Stage	Mineral	Fe	As	S	Ni	Pb	Cu	Ag	Zn	Cd	Au	Sb	Total
Pre-ore stage	Pyrite	45.81	0	52	0.03	0.05	0.57	0.03	0.01	0	0	0.01	98.5
Pre-ore stage	Pyrite	45.34	0	52.84	0	0.05	1.26	0.05	0.03	0	0	0	99.56
Pre-ore stage	Pyrite	46.23	0	52.62	0.01	0.11	0.21	0	0.08	0.02	0	0.05	99.33
Pre-ore stage	Pyrite	45.54	0	52.15	0.01	0.05	0.5	0.03	0.03	0	0	0	98.31
Main Cu stage	Chalcopyrite	29.9	0.04	34.41	0	0.05	34.08	0.07	0.04	0.01	0	0	98.6
Main Cu stage	Chalcopyrite	30.17	0.03	34.46	0.02	0.03	34.59	0.01	0.2	0.02	0.14	0.03	99.69
Main Cu stage	Chalcopyrite	29.93	0	34.86	0.05	0.02	34.69	0.02	0	0	0	0	99.57
Main Cu stage	Chalcopyrite	29.87	0	34.48	0.01	0.03	34.51	0.03	0.06	0	0.11	0	99.1
Main Cu stage	Sphalerite	0.79	0	32.6	0	0.09	0.6	0.01	66.21	0.38	0.07	0.01	100.76
Main Cu stage	Sphalerite	1.41	0.03	32.94	0.02	0	0.88	0	64.72	0.33	0	0	100.34
Main Ag stage	Argentite	0.21	0	14.29	0	0.03	0.71	83.25	0	0	0	0	98.47
Main Ag stage	Argentite	0.46	0.01	17.26	0	0.08	3.74	78.25	0.06	0.27	0	0	100.12
Main Ag stage	Native silver	0.04	0	0.09	0.01	0	0.14	99.75	0	0.33	0.24	0	100.6
Main Ag stage	Chalcopyrite	29.4	0	34.51	0	0.07	34.95	0.04	0.65	0.02	0	0.01	99.64
Main Ag stage	Chalcopyrite	29.35	0.01	34.01	0.02	0.04	34.5	0	0.75	0	0	0	98.68
Main Ag stage	Chalcopyrite	29.52	0.14	34.33	0.02	0.06	34.44	0.03	0.19	0.03	0.01	0	98.76
Main Ag stage	Chalcopyrite	28.31	0	34.36	0	0.11	34.54	0.02	1.41	0.02	0	0	98.77
Main Ag stage	Chalcopyrite	30.27	0.14	35.1	0.01	0.07	34.64	0.08	0	0	0.13	0	100.42
Main Ag stage	Chalcopyrite	29.48	0	32.74	0.01	0.09	34.34	0.46	0	0.03	0	0	97.14
Main Ag stage	Chalcopyrite	26.01	0.01	32.27	0.02	0.04	29.84	10.57	0.03	0	0	0	98.79
Main Ag stage	Chalcopyrite	27.35	0	34.08	0.01	0.05	31.71	7.98	0	0	0	0.01	101.19
Main Ag stage	Galena	0.03	0	13.16	0	86.16	0	0.03	0.17	0.09	0	0.03	99.68
Main Ag stage	Galena	0.01	0	13.2	0.03	86.42	0	0	0.01	0.01	0.02	0	99.7
Main Ag stage	Galena	0.03	0	13.07	0	86.12	0.03	0.06	0	0.15	0.01	0.02	99.5
Main Ag stage	Galena	0.11	0	13.31	0.07	86.64	0.05	0.01	0	0.14	0.2	0	100.52
Main Ag stage	Galena	0.01	0	13.11	0	86.78	0.4	0.11	0	0.11	0.05	0	100.56
Main Ag stage	Pyrite	46.41	0	53.69	0	0	0	0.02	0.07	0	0	0	100.19
Main Ag stage	Pyrite	47.06	0	52.44	0.01	0	0.01	0.02	0.01	0	0	0	99.54
Main Ag stage	Pyrite	46.92	0	53.32	0	0.05	0.03	0.01	0	0.03	0	0.04	100.39
Main Ag stage	Sphalerite	0.16	0	32.43	0	0.01	0.16	0.05	65.69	0.48	0.04	0.01	99.02
Main Ag stage	Sphalerite	0.37	0	32.89	0	0.13	0.36	0.06	66.36	0.41	0.08	0	100.66
Main Ag stage	Sphalerite	0.41	0	32.83	0	0.02	0.21	0.03	65.01	0.36	0.47	0.01	99.34
Main Ag stage	Sphalerite	0.64	0.05	32.6	0.02	0	1.14	0.11	64.33	0.4	0.04	0.22	99.56
Main Ag stage	Sphalerite	0.33	0.1	32.56	0	0.07	0.01	0	66.08	0.49	0.28	0	99.9

subtype inclusions of similar V/(V + L) ratio and shape occurred isolated (Fig. 9c) or in the growth zones of quartz grains (Fig. 9b). FIA 2 (Fig. 9f) is rare, with most of the FIs randomly or sporadically occurred in quartz or sphalerite grains. All the possible combinations of FIA 2 are seen in the main Cu stage while only the WL + WV assemblage is recognized in the main Ag stage. FIA 3 is commonly seen in every sample in the Yueyang district, and regarded to be secondary in origin as previously indicated.

5.2. Microthermometric results

The microthermometric data of FIs are summarized in Table 3 and Fig. 10.

FIs of the main Cu-stage minerals are mainly WL- and minor WV-, C- and S-type FIs. The WL-subtype FIs, accounting for more than 95% in proportion, yielded ice-melting temperatures ($T_{m,\ ice}$) ranging from −0.1 to −10.5 °C and −2.0 ± 1.7 °C (1σ; n = 154) on average, with corresponding average salinity of 3.3 ± 2.7 wt% NaCl eqv. Most of these FIs homogenized into liquid phase at temperatures of 134–382 °C; but five of them showed critical homogenization, with total homogenization temperatures (Th) ranging from 293 to 377 °C. Overall, the Th ranges from 134 to 382 °C with 259 ± 37 °C (1σ; n = 149) on average, and calculated average density is 0.82 ± 0.07 g/cm^3 (1σ; n = 154). The WV-subtype FIs are rare but recognized as primary in origin as they scatter in the quartz grains and no fissures or microfractures were identified nearby. Only three of them are obtained with reliable microthermometric results due to the vague phase outlines. Their $T_{m,ice}$ are −1.2, −3.3 and −4.8 °C, corresponding to salinities of 2.1, 5.4 and 7.6 wt% NaCl eqv., respectively. They all homogenized into vapor phase at 387, 378 and 372 °C, with corresponding densities of 0.49, 0.60 and 0.66 g/cm^{-3}. Two C-type FIs coexisting with the WV-subtype FIs both yielded solid CO_2 melting temperatures of −56.6 °C, suggesting no other volatile gases in the vapor phase. Their clathrate-melting and total homogenization temperatures are 6.4, 6.5 °C and 422, 351 °C, respectively, yielding corresponding salinities of 6.7 and 6.5 wt% NaCl eqv. and densities of 0.32 and 0.28 g/cm^{-3}. Two S-type FIs, with vapor phase less than 20 vol%, both contain a halite daughter mineral, which dissolved after the disappearance of the vapor bubble at 290 and 275 °C during heating, corresponding to salinities of 37.4 and 36.3 wt% NaCl eqv., and densities of 1.17 and 1.19 g/cm^{-3}, respectively.

The main Ag-stage minerals (quartz and sphalerite) contain abundant WL- and minor WV-subtype FIs. The $T_{m,\ ice}$ of the WL-subtype FIs range from −0.1 to −8.1 °C, corresponding to salinities from 0.2 to 11.8 wt% NaCl eqv. Among the analyzed inclusions, most (134 inclusions) homogenized into liquid upon heating at temperatures ranging from 179 to 363 °C, with only one exceptional inclusion showed critical homogenization at 364 °C. The overall Th range from 179 to 364 °C with an average of 250 ± 38 °C (1σ; n = 135). Eight sets of data of the WV-subtype FIs were obtained (Table 3), with average Th of 350 ± 58 °C and $T_{m,\ ice}$ of −1.5 ± 1.1 °C (1σ), corresponding to average salinities of 2.6 ± 1.7 wt% NaCl eqv. and densities of 0.50 ± 0.02 g/cm^{-3} (1σ).

As for the late stage, only the WL-subtype FIs with less than 20 vol% vapor bubble were observed and yielded average $T_{m,ice}$ of −0.7 ± 0.5 °C and Th of 184 ± 52 °C (1σ; n = 64), with calculated salinities and densities of 1.3 ± 0.8 wt% NaCl eqv. and 0.89 ± 0.06 g/cm^{-3} (1σ; n = 64), respectively.

5.3. Laser Raman spectroscopy analysis

Laser Raman spectroscopy analysis was carried out to reveal the composition of vapor and liquid phases of the main Cu- and Ag-

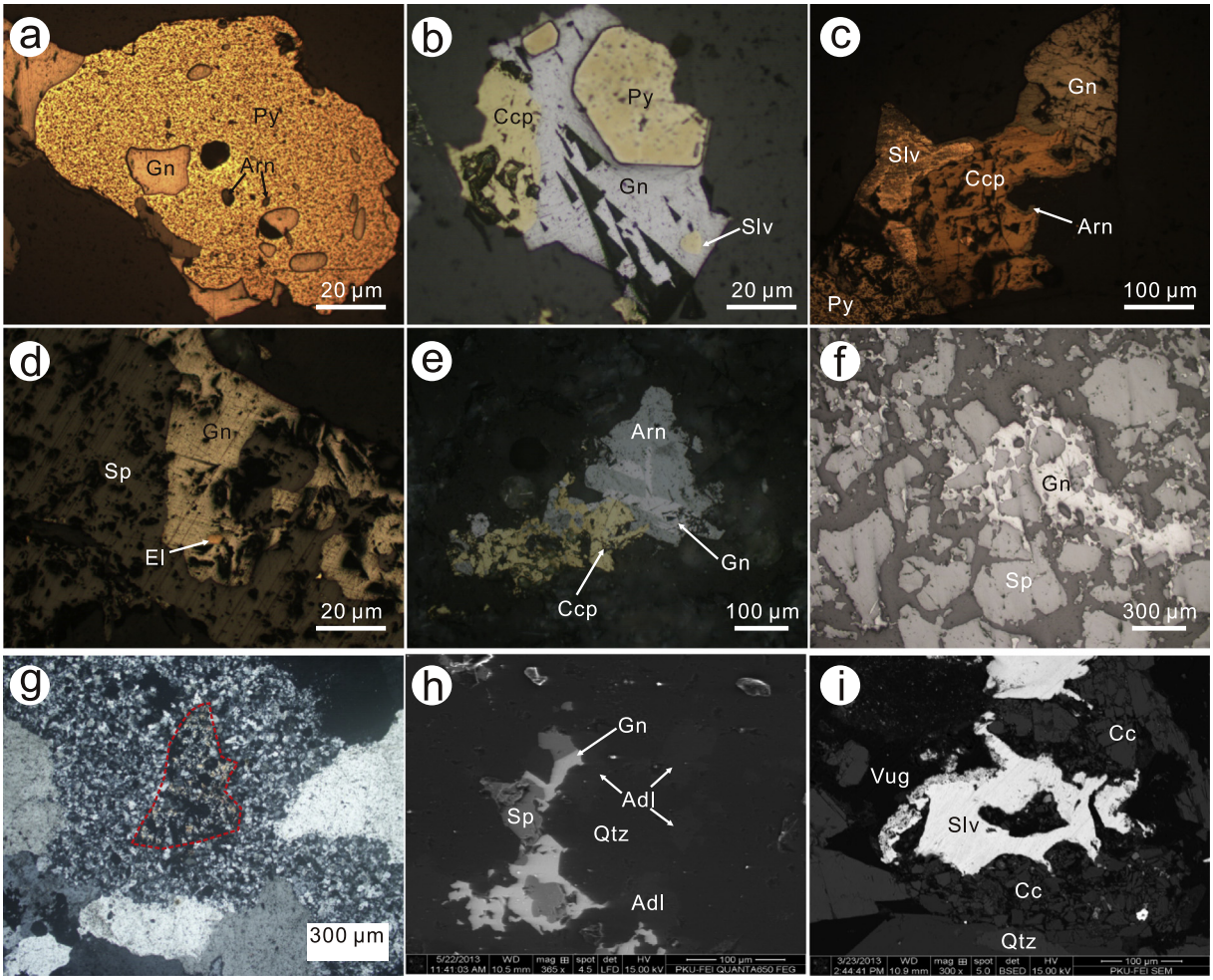

Fig. 8. Photomicrographs showing mineral assemblages and textures of the main Ag stage in the Yueyang Ag-Au-Cu deposit. (a) Large pyrite grains, with galena and argentite inclusions, coexist with large galena grains. (b) Native silver occurs as inclusions in galena, which is intergrown with chalcopyrite and pyrite grains. (c) Native silver, Ag-bearing chalcopyrite, argentite, galena and pyrite coexist in a quartz vein. (d) Minute electrum grain is included in galena, which coexists with sphalerite. (e) Large argentite grain intergrown with galena and chalcopyrite. (f) Typical galena-sphalerite-quartz assemblage in the Pb-Zn massive ore in Fig. 6h. (g) Sericite-pyrite cluster is overprinted and surrounded by fine-grained quartz grains. (h) Adularia grains are intergrown with quartz, sphalerite and galena grains in the Ag-bearing veins (back-scatter electron image). (i) Native silver and calcite grains fill in the cavities between euhedral quartz grains (backscatter electron image). Abbreviations: Arn, argentite; Ccp, chalcopyrite; El, electrum; Py, pyrite; Gn, galena; Sp, sphalerite; Slv, native silver; Adl, adularia; Cc, calcite; Qtz, quartz.

stage FIs. The vapor and liquid phases of the W-type FIs hosted in most quartz and sphalerite crystals are dominated by H_2O (Fig. 11a), while minor amounts of CO_2 can only be identified in the vapor in some inclusions, indicated by a CO_2 peak (1388 cm^{-1}) (Fig. 11b), but the CO_2 contents in the vapor are too low to form clathrates even upon cooling. In the C-type FIs, the vapor phase is dominated by CO_2 with two peaks of 1284 and 1388 cm^{-1} (Fig. 11c). Besides CO_2 and H_2O, other gases are not detected in the Yueyang district, which is consistent with the results of the microthermometric analyses.

6. Hydrogen and oxygen isotopic compositions

The hydrogen and oxygen isotopic composition of silica phases (euhedral to sub-euhedral quartz) and fluid inclusions at Yueyang deposit were used to identify the sources of ore-forming fluids and to infer the evolution process of the system. Temperatures used for calculation of $\delta^{18}O_{H2O}$ from $\delta^{18}O_Q$ are average Th of each sample (for those with microthermometric results) or each stage (for those without). Petrologic characteristics of 11 samples analyzed for δD and $\delta^{18}O$ isotopic study were briefly introduced in Table 4. The δD_{H2O} values of the two main Cu-stage samples (Y-04a, Y-14) are −64‰ and −62‰, while the $\delta^{18}O_Q$ values are 11.1‰ and 11.8‰, corresponding to calculated $\delta^{18}O_{H2O}$ of 2.3‰ and 2.7‰, respectively. Both the δD_{H2O} and $\delta^{18}O_{H2O}$ values of the two samples are nearly identical, and plot adjacent to the box of magmatic water in the δD vs. $\delta^{18}O$ plot (Fig. 13), indicating a possible magmatic origin. δD_{H2O}, $\delta^{18}O_Q$ and $\delta^{18}O_{H2O}$ values of seven samples from the main Ag stage varied from −81‰ to −63‰, 7.8‰ to 9.1‰ and −5.5‰ to 0.2‰, respectively. The δD_{H2O} and $\delta^{18}O_{H2O}$ values of two late-stage samples are −64‰, −71‰ and −3.2‰, −8.5‰, which are close to the Jurassic–Cretaceous meteoric water in Southwest Fujian Province (Zhang, 1985; Fig. 13).

7. Discussion

7.1. Origin of the ore-forming fluids

Two main Cu-stage samples plot adjacent to the box of primary magmatic water in the δD vs. $\delta^{18}O$ plot (Fig. 13), indicating that the ore-forming fluid of the main Cu stage is magmatic-dominated in origin, with no input of meteoric water. This deduction is also supported by the high-temperature (average Th of 381 °C), low-density (0.48–0.66 g/cm^{-3}), but varying salinity (0.4–7.6 wt% NaCl

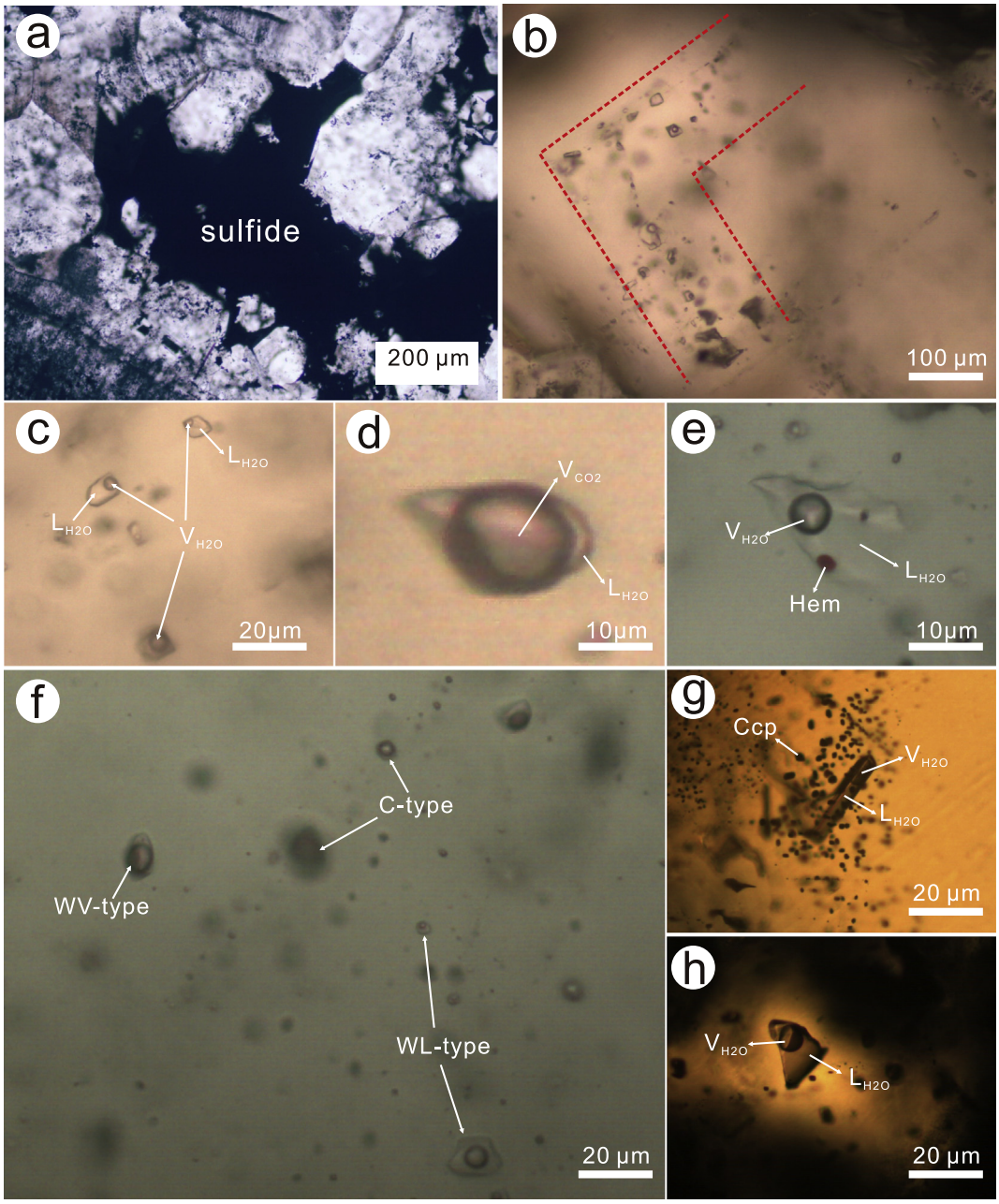

Fig. 9. Photomicrographs of fluid inclusions of the Yueyang deposit. (a) Sulfides occupy the intergranular spaces between euhedral quartz grains, indicating a co-depositional relationship. (b) Primary fluid inclusions occur in the growth zone of euhedral coarse-grained quartz in the main Ag stage. (c) WL-subtype inclusions in quartz. (d) C-type inclusion in quartz of the main Cu stage. (e) S-type inclusion with a hematite and unknown black daughter minerals. (f) WV + WL + C FIA in quartz of the main Cu stage. (g) Minute chalcopyrite and WL-subtype inclusions in the main Ag-stage sphalerite. (h) WL-subtype inclusion in sphalerite. *Abbreviations:* L_{H2O}, H_2O liquid; V_{H2O}, H_2O vapor; V_{CO2}, CO_2 vapor; Ccp, chalcopyrite; Hem, hematite.

Table 3
Microthermometric data of FIs in quartz and sphalerite from the Yueyang Ag-Au-Cu deposit.*

Stage	Type	Num.	T_h (°C)	$T_{m,ice}$ (°C)	$T_{m,cla}$ (°C)	T_{mNaCl} (°C)	Salinity (wt% NaCl)	Density (g/cm^3)
Main Cu	WL	154	259 ± 37	−2.0 ± 1.7			3.3 ± 2.7	0.82 ± 0.07
Stage	WV	3	379 ± 7	−3.0 ± 2.0			5.0 ± 2.8	0.58 ± 0.08
	C	2	351, 422		6.4, 6.5		6.7, 6.5	0.32, 0.28
	S	2	290, 275			290, 275	37.4, 36.3	1.17, 1.19
Main Ag	WL	135	250 ± 38	−1.3 ± 1.2			2.2 ± 1.9	0.83 ± 0.08
Stage	WV	8	350 ± 58	−1.5 ± 1.1			2.6 ± 1.7	0.50 ± 0.02
Late stage	WL	64	184 ± 52	−0.7 ± 0.5			1.3 ± 0.8	0.89 ± 0.06

Abbreviations: T_h, homogenization temperature; $T_{m,ice}$, ice-melting temperature; $T_{m,cla}$, clathrate melting temperature; $T_{m,NaCl}$, halite dissolution temperature.
* All the data are in 1σ deviation.

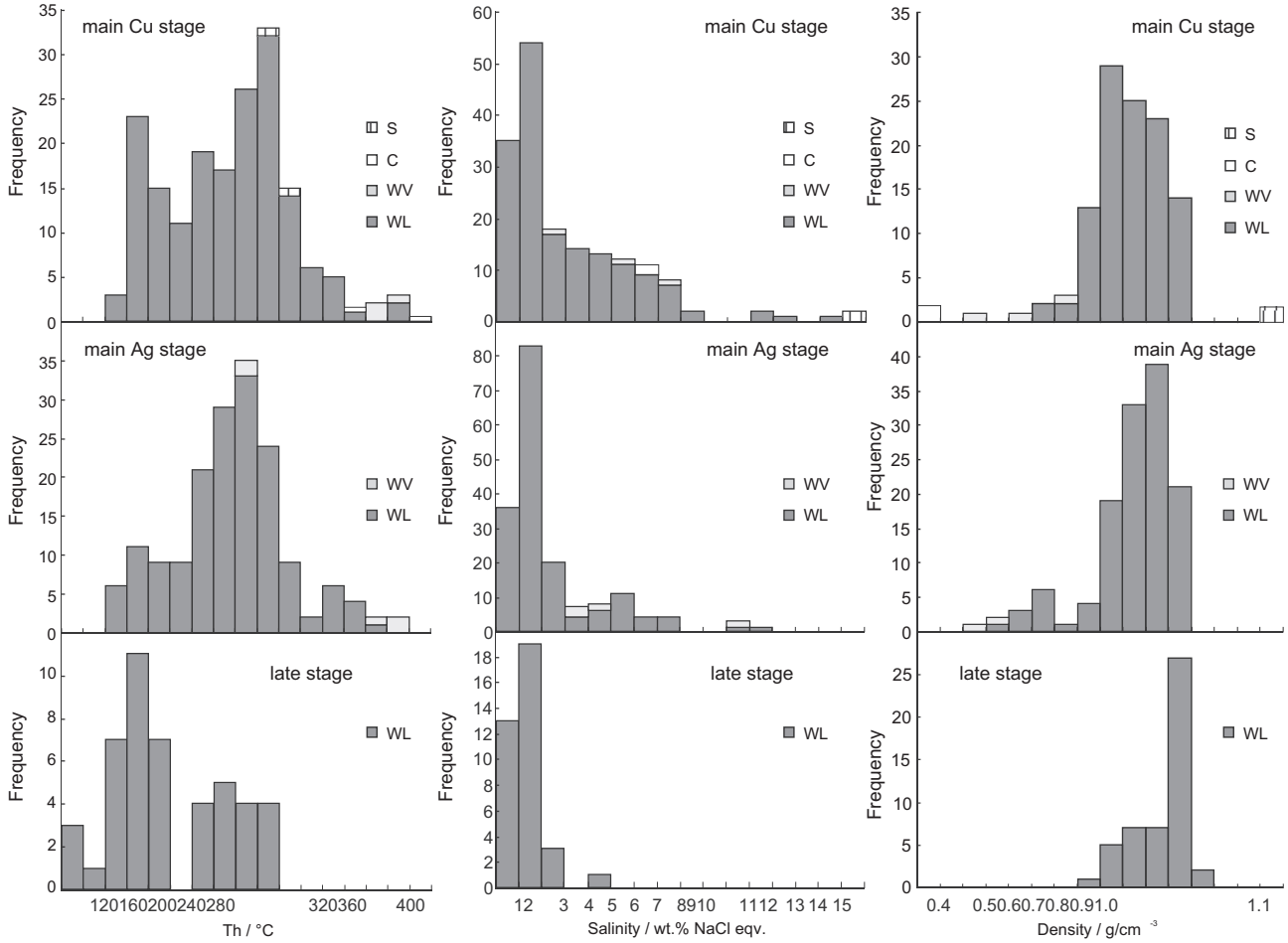

Fig. 10. Histograms of homogenization temperatures, salinities and densities of FIs in different stages of the Yueyang Ag-Au-Cu deposit.

eqv.) C- and WV-subtype FIA of the main Cu stage, especially in sample Y-11. They were commonly identified and regarded as the separation from the boiling assemblage in the lower parts of other low-sulfidation epithermal deposits or geothermal systems, such as the Broadlands-Ohaaki, Zunil and Los Azufres (Hedenquist and Henley, 1985; Moore et al., 1992; Simmons et al., 2007).

High Th (>300 °C) WV + WL inclusion assemblage is identified in native silver-bearing vein sample Y-02 of the main Ag stage, which resembles those high-temperature FIA in the main Cu stage. However, the C-type and S-type FIs are absent, and most of the inclusions homogenized at temperatures below 300 °C, implying a meteoric water-dominated origin for the main Ag stage. Moreover, the main Ag-stage samples plot between the magmatic water box and meteoric water line, but closer to the latter in the δD-$\delta^{18}O$ diagram (Fig. 13), which also supported the meteoric-dominated origin for the main Ag-stage ore-forming fluids. The data locations of the main Ag-stage samples could also be resulted from the water-rock interaction between the deeply circulated meteoric water and wallrocks—the "^{18}O-shift" (Craig, 1963; Taylor, 1974). Both the explanations of the D-O isotope systems indicated that the ore-forming fluids of the main Ag stage were meteoric water in source, possibly with nil input of magmatic components.

The ore-forming fluids of the post-ore stage are totally meteoric water-dominated, as the two late-stage samples (Y-15 and Y-04b) plot adjacent to the Jurassic–Cretaceous meteoric water in Southwest Fujian (Zhang, 1985). Besides, the meteoric water origin of the late-stage fluids is further supported by the low Th, low salinities of the FIs, and the comb and colloform ore textures.

In general, the ore-forming fluids of the Yueyang deposit evolved from magmatic vapor-dominated for the main Cu stage, through predominant meteoric water with little input of magmatic water in the main Ag stage, to pure meteoric water of the late stage.

7.2. Ore-forming mechanism and fluid evolution

7.2.1. Possible ore component transportation and deposition mechanism

Previous experimental studies have shown that copper chloride complexes are likely to be the most important aqueous species of copper ($CuCl_2$ or $CuCl^+$) in epithermal-porphyry environments (Barns, 1997; Mountain and Seward, 1999; Ulrich et al., 2002; Muntean and Einaudi, 2001). However, silver is mainly transported as hydrosulfide complexes (AgHS, $Ag(HS)_2^-$) in dilute (up to 3.5% wt NaCl eqv.) hydrothermal fluids of meteoric origin (Seward, 1976; Seward and Barns, 1997; Stefánsson and Seward, 2003 and reference therein). In this case, possible copper and silver complex species of the Yueyang deposit would be $CuCl_2$ or $CuCl^+$ and Ag(HS)(aq) or $Ag(HS)_2^-$, respectively.

Fluid boiling (Drummond and Ohmoto, 1985; André-Mayer et al., 2002; Brathwaite and Faure, 2002; Simmons et al., 2007; Canet et al., 2011) and mixing (Faure et al., 2002; Hedenquist et al., 1998) are most conducive to ore mineral precipitation in

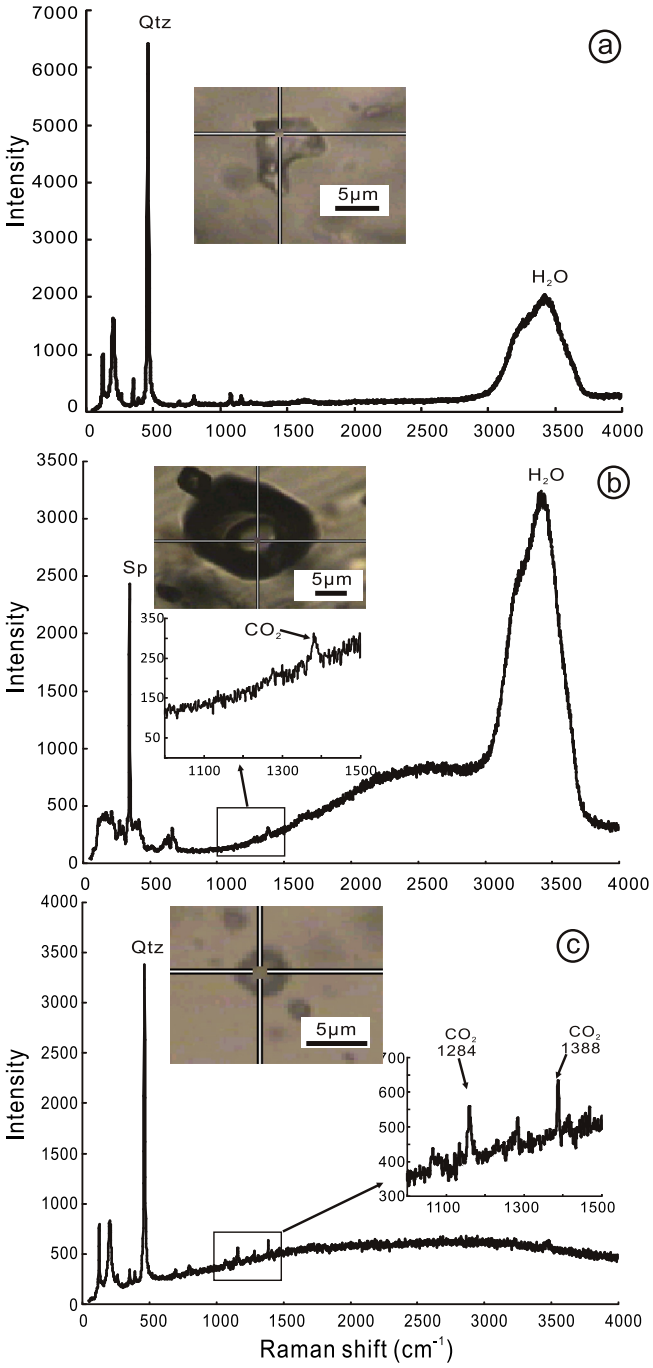

Fig. 11. Laser Raman spectra of fluid inclusions. (a) H_2O-spectrum of the WL-subtype inclusion. (b) CO_2-spectrum of the vapor and H_2O-spectrum of the liquid of the C-type inclusion; (c) CO_2-spectrum of the C-type inclusion.

epithermal systems, as they effectively control compositional changes including pH, Eh, f_{O2}, f_{H2S} and further cause supersaturation and precipitation of ore minerals (Drummond and Ohmoto, 1985; Barns, 1997). Simple cooling of hydrothermal fluids or interaction with surrounding wall rocks, however, seems to be less important in governing ore deposition (Drummond and Ohmoto, 1985; André-Mayer et al., 2002). These processes can be distinguished by mineralogy, ore fabrics and fluid inclusion studies (cf. Hedenquist and Henley, 1985; Simmons et al., 2005; Canet et al., 2011).

Fluid boiling (immiscibility) is important in the main Cu-stage mineralization in the Yueyang deposit, as supported by the following evidences: (1) the WL-, WV-subtype and minor C-type inclusions are observed in a single quartz grain in sample Y-11, with similar Th but contrasting salinities; (2) the WL-subtype FIs in most main Cu-stage samples show a broad range in salinity from 0.4 to 14.5 wt% NaCl eqv. with similar Th, and (3) hydrothermally brecciated texture is common in the main Cu stage.

Besides fluid boiling, fluid mixing process is also identified in the main Cu stage, especially in sample Y-04 and Y-14. FIs from these samples can be classified into a relatively high-salinity (>3 wt% NaCl eqv.) and low-salinity (<2 wt% NaCl eqv.) groups (Fig. 12), and those with higher salinities show distinct mixing trend as their salinities and Th are in positive correlations (Fig. 12). The D-O isotopic systems also indicated that fluid mixing occurred during the main Cu stage.

In the main Ag stage, both the C-type FIs and brecciated texture are absent, but FIA 3 (WL- and WV-subtype FIs) representing fluid immiscibility is observed. Besides, in those samples containing only the WL-subtype inclusions yielded similar homogenization temperatures but contrasting salinities (e.g., $160B_1$), and an increasing trend of the salinity as the Th decreases can be observed (Fig. 12), which both indicated that fluid immiscibility without significant vapor/gas release occurred (Simmons and Browne, 1997; Hedenquist and Henley, 1985; Canet et al., 2011). In addition, adularia and calcite grains are identified in the native silver-bearing quartz veins (Fig. 8h), which were commonly suggested to have resulted from fluid boiling in low-sulfidation systems (Simmons et al., 2005; Canet et al., 2011).

Cooling of ore-forming fluids is common under ~200 °C as shown in Fig. 12 (e.g., Y-03). This process is further supported by relatively simple mineral composition (predominant quartz crystals) and their crystal morphologies (coarse-grained, euhedral). However, both Cu and Ag mineralization barely resulted from this process as only minor chalcopyrite grains were discovered in those euhedral quartz grains and scarce native silver inclusions in galena or sphalerite (Fig. 8b).

7.2.2. Fluid evolution processes

On the basis of the abovementioned ore fabrics, fluid inclusion and D-O stable isotope studies, it is suggested that the relatively high-temperature (>200 °C) ore-forming fluid of the main Cu stage was magmatic vapor-dominated. Fluid boiling and further mixing with low-temperature, low-salinity meteoric water resulted in the decrease of both the temperature and Cl contents of the ore-forming fluid, which further caused the instability of copper chloride complexes and the precipitation of chalcopyrite.

The ore-forming fluid of the main Ag stage evolved into a meteoric water-dominated, with fluid boiling widely recognized. The fluid boiling process would release much of the residual vapor in hydrothermal fluid and cause the instability of hydrosulfide complexes of silver and precipitation of Ag-bearing minerals in the forms of Ag-rich chalcopyrite and native silver (Fig. 8c). Besides, the early precipitation of other sulfides (pyrite, galena, sphalerite) would also promote H_2S decrease in solution, thereby causing argentite or electrum to precipitate in the growing sulfide crystals (Fig. 8a, b, d). The continued consumption of H_2S and CO_2 would also cause a pH increase of the solution, and concomitant precipitation of adularia and calcite (André-Mayer et al., 2002; Canet et al., 2011), which are only observed in the main Ag stage in Yueyang deposit. After pervasive fluid boiling, minor amounts of Ag and Cu minerals were precipitated by simple cooling of the ore-forming fluids, but of much less significance.

The ore-forming fluids of the late stage are low-temperature, low-salinity meteoric water, and the formation of barren calcite-quartz or amethyst veins marks the termination of the low-sulfidation epithermal mineralization system.

Table 4
The $\delta^{18}O$ and δD ratios (‰) for the Yueyang Ag-Au-Cu deposit.

Sample No.	Mineralization stage	Sample description	δD_{H2O} (‰)	$\delta^{18}O_Q$ (‰)	Th (°C)	$\delta^{18}O_{H2O}$ (‰)
Y-14	Main Cu stage	Massive Qtz-Ccp-Py-Sp-Gn ore	−62	11.8	247	2.7
Y-04a	Main Cu stage	Massive Qtz-Ccp-Py ore	−64	11.1	253	2.3
Y-03	Main Ag stage	(drusy) Qtz-Ccp-Py vein	−75	8	174	−5.5
Y-06	Main Ag stage	Qtz-Sp-Gn-Ccp vein	−63	7.8	201	−3.8
Y-08	Main Ag stage	Qtz-Sp-Gn-Py vein	−77	8.8	250	−0.1
Y-13	Main Ag stage	Qtz-Sp-Gn-Py vein	−75	8.5	250	−0.4
−100B	Main Ag stage	Massive silicic Ag-bearing ore	−67	8.2	250	−0.7
130-3	Main Ag stage	Massive silicic Ag-bearing ore	−74	9.1	250	0.2
160-11	Main Ag stage	Massive silicic Ag-bearing ore	−81	7.5	250	−1.4
Y-04b	Late stage	Barren Qtz-Cc vein	−64	9.6	184	−3.2
Y-15	Late stage	Barren Qtz vein	−71	8.4	135	−8.5

Abbreviations: Cc, calcite; Ccp, chalcopyrite; Gn, galena; Py, pyrite; Qtz, quartz; Sp, sphalerite.

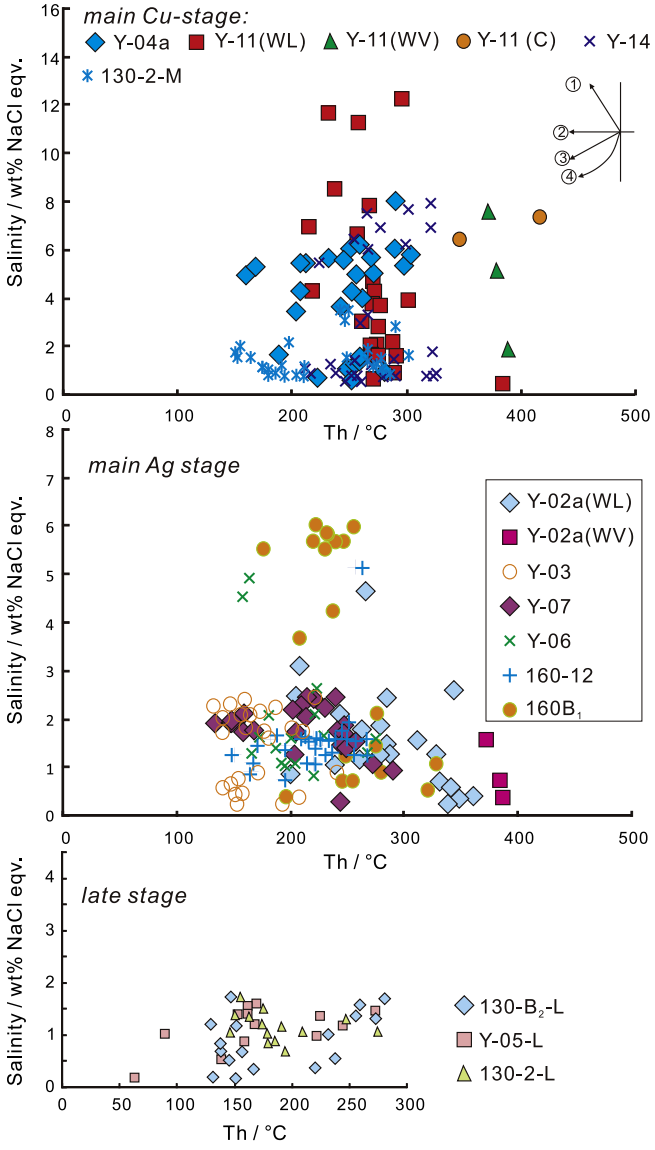

Fig. 12. Homogenization temperatures vs. salinities of fluid inclusions in different stages.

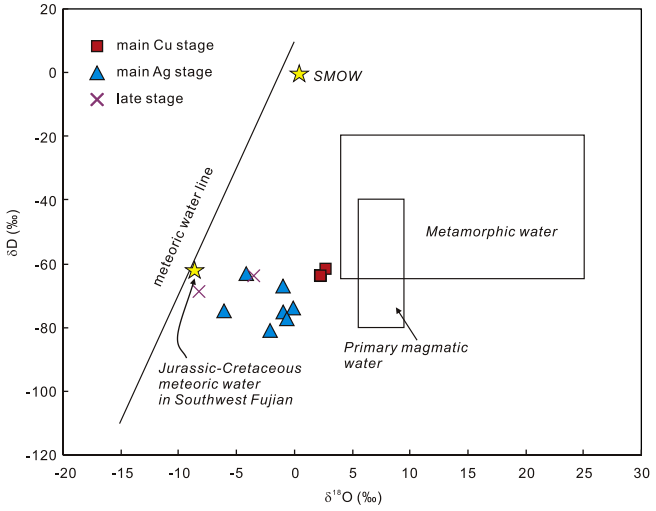

Fig. 13. The $\delta D-\delta^{18}O$ systematics for the Yueyang Ag-Au-Cu deposit (after Taylor, 1974).

7.3. Trapping pressure and mineralization depth

Most of the main Cu-stage and nearly all the main Ag-stage samples underwent fluid boiling. Consequently, it is not necessary to make a pressure correction to the measured homogenization temperatures. Furthermore, trapping pressures of these inclusions can be obtained by boiling-point curves for H_2O-NaCl systems (Haas, 1971). Average Th and salinities of every stage (Table. 3) were used for pressure estimation. We utilized Haas' (1971) diagram and interpolated the possible depth of each mineralization stage between 2.0 and 5.0 wt% NaCl eqv., and they are 448 and 527 m for main Ag and Cu stage, respectively (Fig. 14). The current average land surface elevation of the Yueyang basin is ~300 m, thus the orebodies from −100 m to −160 m in elevation (−130 m in average) are situated nearly 430 m underground in average. This is nearly identical and only 100 m shallower than the formation depth of the main Ag and main Cu stage, respectively. In other words, the Yueyang deposit underwent much less uplift and exhumation since its formation than the Zijinshan Cu-Au (~500 m, So et al., 1998) and Luoboling Cu-Mo deposit (~1 km in minimum, Zhong et al., 2014) to the northeast, which is consistent with less volcanic rock occurrences from southwest to northeast in the district (Fig. 1). Therefore, the possible low-sulfidation epithermal deposits could be found in the southwest while more porphyry deposits in the northeast of the Zijinshan orefield.

The average mineralization depth of main Cu stage is 79 m deeper than that of the main Ag stage, which is inconsistent to the spacial distribution that the Cu orebodies are shallower than Ag orebodies. Hedenquist and Henley (1985) confirmed that CO_2 would decrease the depth of boiling in epithermal systems, which is the possible reason for depth differences of the Yueyang deposit.

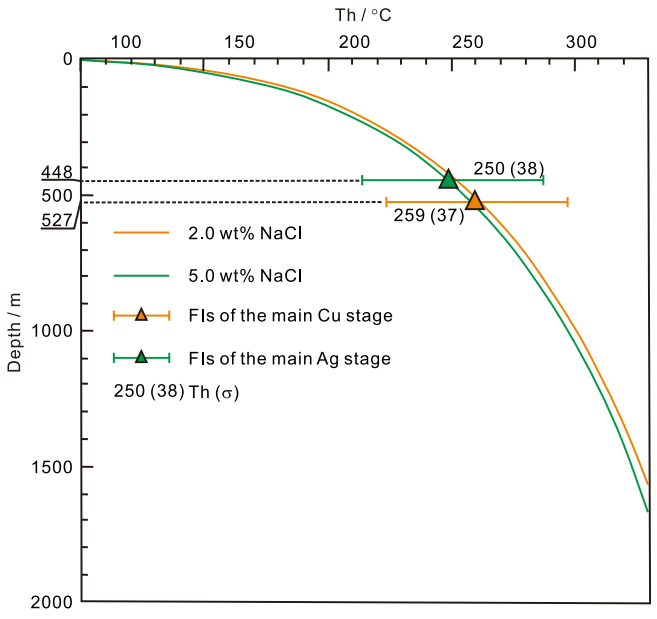

Fig. 14. Pressure estimation for the Yueyang Ag-Au-Cu deposit. Boiling-depth curves for NaCl-H_2O solutions are from Haas (1971). Average homogenization temperatures and salinities of the main Cu and Ag stage are used for depth estimation.

7.4. Two-stage mineralization event in the Yueyang deposit

On the basis of the aforementioned geological, fluid inclusion and stable isotope studies, a two-stage mineralization model in the Yueyang deposit is proposed (Fig. 15). The first-stage mineralization is the porphyry type Cu mineralization although the mineralization scale is limited (less than 40,000 t Cu). It is attributed to the buoyant magmatic vapor escaped from a porphyry mineralization system beneath, and characterized by the brecciated ore textures, sericite alteration, the occurrence of the vapor-rich C-type and WV-type inclusions with high total homogenization temperatures, and magmatic origin of the ore-forming fluids. The second-stage mineralization is the typical low-sulfidation epithermal Ag-Au-Cu mineralization. It is the predominant mineralization type in the Yueyang deposit and genetically related to the evolution of meteoric water. The representative features include the crustiform and colloform ore textures, adularia-carbonate alteration, the presence of WL-type inclusions with low total homogenization temperatures (mostly < 300 °C), and the fluid source of meteoric water.

The coexistence of the porphyry type Cu and epithermal Ag-Au-Cu mineralization in the Yueyang deposit might be caused by: (1) the systematic waning history of a porphyry-epithermal mineralization system; and (2) the telescoping of a later epithermal mineralization event onto an earlier porphyry type mineralization event. It seems that the telescoping model might be more suitable since the reported sericite Ar^{40}–Ar^{39} age for the sericite alteration (related to Cu mineralization) in the Yueyang deposit (102.9 ± 1.9 Ma (Zhang et al., 2003b) is ~10 Ma older than the adularia (related to Ag-Au mineralization) Ar^{40}–Ar^{39} ages (~95 Ma–91 Ma, Zhang et al., 2003a; Liu and Hua, 2005), signifying two separate mineralization events. However, more precise age and other direct evidences are needed to further support the telescoping model as both the sample description and the relationship between the sericite sample and Cu mineralization were not mentioned by Zhang et al. (2003b), although only one phyllic alteration event was recognized in the Yueyang deposit.

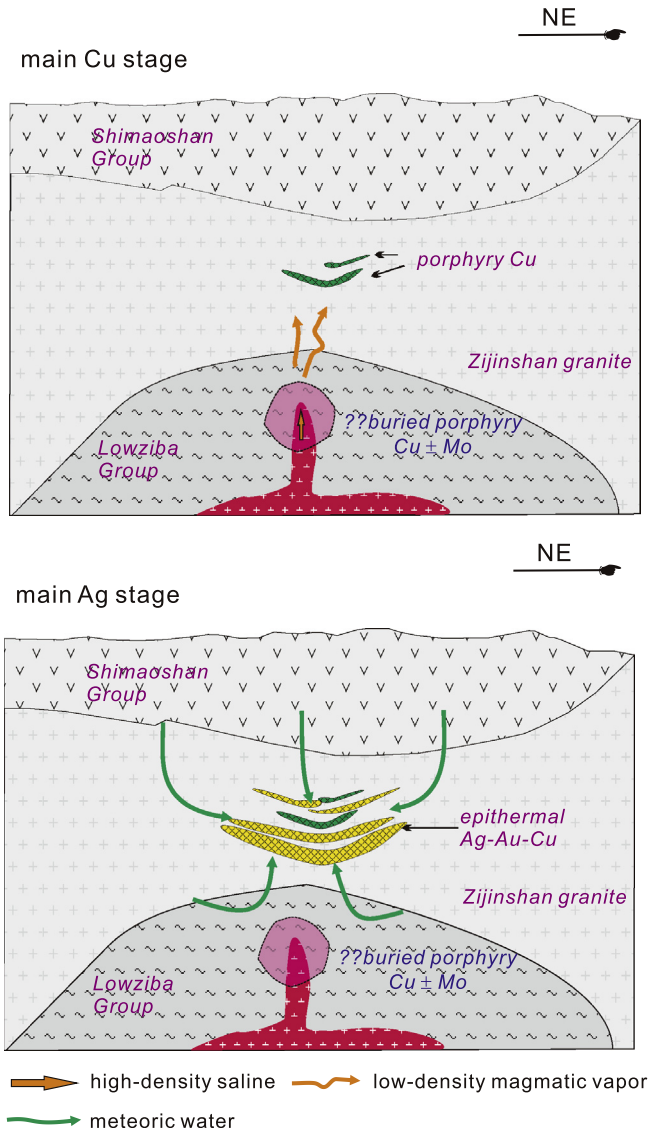

Fig. 15. Two-stage mineralization model in the Yueyang Au-Ag-Cu deposit (not to scale, see text for discussion).

8. Concluding remarks

(1) Four mineralization stages are recognized in the Yueyang low-sulfidation epithermal Ag-Au-Cu deposit, namely: pre-ore, main Cu, main Ag and post-ore stages. Mineral assemblages of each stage are sericite + pyrite + quartz ± chorite, chalcopyrite + pyrite + sericite + quartz ± illite ± bornite, Ag (Au)-bearing ore minerals + pyrite + quartz ± adularia ± calcite ± apatite ± chalcopyrite ± galena ± sphalerite, and quartz ± chalcedony ± calcite, respectively.

(2) The ore-forming fluids of the main Cu stage are magmatic vapor-dominated, with fluid boiling and mixing both the possible ore-precipitation mechanisms. The ore-forming solutions of the main Ag stage, however, are predominantly meteoric water in origin. The decline of H_2S activity resulted from fluid boiling and precipitation of other sulfides is the possible mechanism of Ag-Au mineral formation.

(3) The mineralization depths of the Cu and Ag-Au orebodies are estimated to be ~527 m and 448 m, respectively. By comprehensive studies of the uplift and exhumation history in

the Zijinshan orefield, it is suggested that more epithermal deposits could be found in the southwest of the orefield, while more porphyry type ones might be expected in the northeast of the orefield.

(4) A two-stage model is proposed for the Yueyang deposit, including an early porphyry type Cu mineralization and a late epithermal Ag-Au-Cu mineralization, although the porphyry type Cu mineralization is very limited in scale.

Acknowledgments

This study is financially supported by the National Natural Science Foundation of China (No. 41502083) and Ministry of Science and Technology of China (No. 2009BAB43B04). The field work is strongly supported by the Zijin Mining Co. Ltd. Drs. Hongrui Fan, Yachun Cai, Xiaochun Li, Defan Wan and Zengjie Zhang assisted the analytical work. Drs. Richen Zhong and Yongfei Yang are thanked for their instructive discussions and suggestions. Constructive suggestions and relevant comments from Editor-in-Chief Franco Pirajno and two anonymous reviewers greatly improved the quality of the paper.

References

André-Mayer, A., Leroy, J., Bailly, L., Chauvet, A., Marcoux, E., Grancea, L., Llosa, F., Rosas, J., 2002. Boiling and vertical mineralization zoning: a case study from the Apacheta low-sulfidation epithermal gold-silver deposit, southern Peru. Miner. Deposita 37, 452–464.

Barns, T.M., 1997. Geochemistry of Hydrothermal Ore Deposits. John Wiley and Sons Inc, New York, p. 972.

Bodnar, R.J., 1993. Revised equation and table for determining the freezing-point depression of H_2O-NaCl solutions. Geochim. Cosmochim. Acta 57, 683–684.

Brathwaite, R.L., Faure, K., 2002. The Waihi epithermal gold-silver-base metal sulfide-quartz vein system, New Zealand: temperature and salinity controls on electrum and sulfide deposition. Econ. Geol. 97, 269–290.

Brown, P.E., 1989. Flincor – a microcomputer program for the reduction and investigation of fluid-inclusion data. Am. Mineral. 74, 1390–1393.

Canet, C., Franco, S.I., Prol-Ledesma, R.M., González-Partida, E., Villanueva-Estrada, R.E., 2011. A model of boiling for fluid inclusion studies: application to the Bolanos Ag-Au-Pb-Zn epithermal deposit, Western Mexico. J. Geochem. Explor. 110, 118–125.

Chang, Z.S., Hedenquist, J.W., White, N.C., Cooke, D.R., Roach, M., Deyell, C.L., Garcia, J., Gemmell, J.B., McKnight, S., Cuison, A.L., 2011. Exploration tools for linked porphyry and epithermal deposits: example from the Mankayan intrusion-centered Cu-Au District, Luzon, Philippines. Econ. Geol. 106, 1365–1398.

Chen, D.F., Han, X.L., Na, J.G., Zhong, T.D., 1997a. Ag-bearing chalcopyrite in the Bitian copper-gold-silver deposit, Fujian Province. Geol. Rev. 43, 529–534 (in Chinese with English abstract).

Chen, D.F., Na, J.G., Zhong, T.H., 1997b. Studies of metallic minerals from the Bitian copper-gold-silver deposit in Fujian Province. Acta Petrol. Miner. 16, 260–268 (in Chinese with English abstract).

Chen, J., 2013. Geological Features, Ore-forming Process of Epithermal Fluid Reformed Copper Deposit Systems in the Zijinshan Orefield, Fujian, China (Master Dissertation). Peking University, Beijing, pp. 1–75 (in Chinese with English abstract).

Chen, J., Chen, Y.J., Zhong, J., Sun, Y., Li, J., Qi, J.P., 2011. Fluid inclusion study of the Wuziqilong Cu deposit in the Zijinshan ore field, Fujian Province. Acta Petrol. Sin. 27, 1425–1438 (in Chinese with English abstract).

Chen, J., Chen, Y.J., Zhong, J., Sun, Y., Qi, J.P., Li, J., 2015. Geological and ore-fluid characteristics of Longjiangting Cu deposit in Zijinshan orefield, Fujian Province, and their genetic implications. Miner. Deposits 34, 98–118 (in Chinese with English abstract).

Chen, Y.J., Ni, P., Fan, H.R.F.P., Lai, Y., Su, W.C., Zhang, H., 2007. Diagnositic fluid inclusions of different types hydrothermal gold deposits. Acta Petrol. Sin. 23, 2085–2108 (in Chinese with English abstract).

Chen, Y.J., Pirajno, F., Wu, G., Qi, J.P., Xiong, X.L., 2012. Epithermal deposits in North Xinjiang, NW China. Int. J. Earth Sci. 101, 889–917.

Chouinard, A., Williams-Jones, A.E., Leonardson, R.W., Hodgson, C.J., Silva, P., Tellez, C., Vega, J., Rojas, F., 2005. Geology and genesis of the multistage high-sulfidation epithermal Pascua Au-Ag-Cu deposit, Chile and Argentina. Econ. Geol. 100, 463–490.

Collins, P.L.F., 1979. Gas hydrates in CO_2-bearing fluid inclusions and the use of freezing data for estimation of salinity. Econ. Geol. 74, 1435–1444.

Clayton, R.N., Mayeda, T.K., 1963. The use of bromine pentafluoride in the extraction of oxygen from oxides and silicates for isotopic analysis. Geochim. Cosmochim. Acta 27, 43–52.

Clayton, R.N., O'Neil, J.L., Meyeda, T.K., 1972. Oxygen isotope exchange between quartz and water. J. Geophys. Res. 77, 3057–3067.

Craig, H., 1963. The Isotopic Geochemistry of Water and Carbon in Geothermal Areas: Nuclear Geology of Geothermal Areas. Consiglio Nazionale della Richerche, Laboratorio de Geologia Nucleare, Spoleto, Pisa, pp. 17–53.

Drummond, S.E., Ohmoto, H., 1985. Chemical evolution and mineral deposition in boiling hydrothermal systems. Econ. Geol. 80, 126–147.

Faure, K., Matsuhisa, Y., Metsugi, H., Mizota, C., Hayashi, S., 2002. The Hishikari Au-Ag epithermal deposit, Japan: oxygen and hydrogen isotope evidence in determining the source of paleohydrothermal fluids. Econ. Geol. 97, 481–498.

Goldstein, R.H., 2001. Fluid inclusions in sedimentary and diagenetic systems. Lithos 55, 159–193.

Goldstein, R.H., Reynolds, T.J., 1994. Systematic of fluid inclusions in diagenetic materials. Soc. Sediment. Geol. Short Course 31, 199.

Haas, J.L., 1971. Effect of salinity on maximum thermal gradient of a hydrothermal system at hydrostatic pressure. Econ. Geol. 66, 940–946.

Hedenquist, J.W., 1987. Mineralization associated with volcanic-related hydrothermal systems in the Circum-Pacific basin. In: Transactions of the Fourth Circum Pacific Conference on Energy and Mineral Resources Conference. American Association of Petroleum Geologists, Singapore, pp. 513–524.

Hedenquist, J.W., Arribas, A., Reynolds, T.J., 1998. Evolution of an intrusion-centered hydrothermal system: far Southeast-Lepanto porphyry and epithermal Cu-Au deposits, Philippines. Econ. Geol. 93, 373–404.

Hedenquist, J.W., Henley, R.W., 1985. The importance of CO_2 on freezing-point measurements of fluid inclusions – evidence from active geothermal systems and implications for epithermal ore deposition. Econ. Geol. 80, 1379–1406.

Hedenquist, J.W., Lowenstern, J.B., 1994. The role of magmas in the formation of hydrothermal ore-deposits. Nature 370, 519–527.

Huang, W.T., Li, J., Liang, H.Y., Wang, C.L., Lin, S.P., Wang, X.Z., 2013. Zircon LA-ICP-MS U-Pb ages and highly oxidized features of magma associated with Luoboling porphyry Cu-Mo deposit in Zijinshan ore field, Fujian Province. Acta Petrol. Sin. 29, 283–293 (in Chinese with English abstract).

Jiang, S.H., Liang, Q.L., Bagas, L., Wang, S.H., Nie, F.J., Liu, Y.F., 2013. Geodynamic setting of the Zijinshan porphyry–epithermal Cu–Au–Mo–Ag ore system, SW Fujian Province, China: constrains from the geochronology and geochemistry of the igneous rocks. Ore Geol. Rev. 53, 287–305.

John, D.A., 2001. Miocene and early Pliocene epithermal gold-silver deposits in the Northern Great Basin, Western United States: characteristics, distribution, and relationship to magmatism. Econ. Geol. 96, 1827–1853.

John, D.A., Hofstra, A.H., Fleck, R.J., Brummer, J.E., Saderholm, E.C., 2003. Geologic setting and genesis of the Mule Canyon low-sulfidation epithermal gold-silver deposit, north-central Nevada. Econ. Geol. 98, 425–463.

Lin, Q.S., 2006. On the characteristics and genesis of the Yueyang silver polymetallic deposit in Wuping County, Fujian Province. Geol. Fujian 25, 82–88 (in Chinese with English abstract).

Liu, W.Y., Cook, N.J., Ciobanu, C.L., Liu, Y., Qiu, X.P., Chen, Y.C., 2016. Mineralogy of tin-sulfides in the Zijinshan porphyry-epithermal system, Fujian Province, China. Ore Geol. Rev. 72, 682–698.

Liu, X.D., Hua, R.M., 2005. ^{40}Ar-^{39}Ar dating of adularia from the Bitian gold-silver-copper deposit, Fujian Province. Geol. Rev. 51, 151–155 (in Chinese with English abstract).

Mao, J.R., Tao, K.Y., Li, J.Y., Xie, F.G., Xu, N.Z., 2002. Geochronology and geochemical characteristics in late Mesozoic Sifang pluton, southwestern Fujian, and their significance. Acta Petrol. Sin. 18, 449–458 (in Chinese with English abstract).

Moore, J.N., Adams, M.C., Lemieux, M.M., 1992. The formation and distribution of CO_2-enriched fluid inclusions in epithermal environments. Geochim. Cosmochim. Acta 56, 121–135.

Mountain, B.W., Seward, T.M., 1999. The hydrosulphide sulphide complexes of copper(I): experimental determination of stoichiometry and stability at 22 °C and reassessment of high temperature data. Geochim. Cosmochim. Acta 63, 11–29.

Muntean, J.L., Einaudi, M.T., 2001. Porphyry-epithermal transition: Maricunga Belt, Northern Chile. Econ. Geol. 96, 743–772.

Roedder, E., 1984. Fluid inclusions. Rev. Mineral. 12, 12–25.

Seward, T.M., 1976. The stability of chloride complexes of silver in hydrothermal solutions up to 350 °C. Geochim. Cosmochim. Acta 40, 1329–1341.

Seward, T.M., Barns, H.L., 1997. Metal transport by hydrothermal ore fluids. In: Barnes, H.L. (Ed.), The Geochemistry of Hydrothermal Ore Deposits. third ed. John Wiley and Sons Inc, New York, pp. 435–486.

Simmons, S.F., Browne, P.R.L., 1997. Saline fluid inclusions in sphalerite from the Broadlands-Ohaaki geothermal system: a coincidental trapping of fluids being boiled toward dryness. Econ. Geol. 92, 485–489.

Simmons, S.F., Simpson, M.P., Reynolds, T.J., 2007. The significance of clathrates in fluid inclusions and the evidence for overpressuring in the Broadlands-Ohaaki geothermal system, New Zealand. Econ. Geol. 102, 127–135.

Simmons, S.F., White, N.C., John, D.A., 2005. Geological Characteristics of Epithermal Precious and Base Metal Deposits. Econ. Geol. 100th Anniversary Volume, pp. 485–522.

Simon, G., Kesler, S.E., Russell, N., Hall, C.M., Bell, D., Pinero, E., 1999. Epithermal gold mineralization in an old volcanic arc: the Jacinto deposit, Camaguey district, Cuba. Econ. Geol. 94, 487–506.

So, C.S., Zhang, D.Q., Yun, S.T., Li, D.X., 1998. Alteration-mineralization zoning and fluid inclusions of the high sulfidation epithermal Cu-Au mineralization at Zijinshan, Fujian Province, China. Econ. Geol. 93, 961–980.

Stefánsson, A., Seward, T.M., 2003. Experimental determination of the stability and stoichiometry of sulphide complexes of silver(I) in hydrothermal solutions to 400 °C. Geochim. Cosmochim. Acta 67, 1395–1413.
Stoffregen, R., 1987. Genesis of acid-sulfate alteration and Au-Cu-Ag mineralization at Summitville, Colorado. Econ. Geol. 82, 1575–1591.
Taylor, H.P., 1974. The application of oxygen and hydrogen isotope studies to problems of hydrothermal alteration and ore deposition. Econ. Geol. 69, 843–883.
Ulrich, T., Gunther, D., Heinrich, C.A., 2002. The evolution of a porphyry Cu-Au deposit, based on LA-ICP-MS analysis of fluid inclusions: Bajo de la Alumbrera, Argentina. Econ. Geol. 97, 1888–1920.
Wan, D.F., Fan, T.Y., Tian, S.H., 2005. The chromium analytical technique for hydrogen isotopes. Acta Geosci. Sin. 26 (Suppl.), 35–38 (in Chinese with English abstract).
Wang, Y.S., 2010. Physical and chemical characteristics of the host rocks in controlling the mineralization of the Chinkuashih high-sulfidation gold-copper deposits, northeastern Taiwan. J. Geochem. Explor. 104, 61–68.
Wang, Y.S., Sasaki, M., Sasada, M., Chen, C.H., 1999. Fluid inclusion studies of the Chinkuashih high-sulfidation gold-copper deposits in Taiwan. Chem. Geol. 154, 155–167.
Wilkinson, J.J., 2001. Fluid inclusions in hydrothermal ore deposits. Lithos 55, 229–272.
Wu, L.Y., Hu, R.Z., Qi, Y.Q., Zhu, J.J., 2013. Zircon LA-ICP-MS U-Pb ages and geochemical characteristics of quartz syenite porphyry from Jintonghu deposit in Zijinshan ore field, Fujian Province, South China. Acta Petrol. Sin. 29, 4151–4166 (in Chinese with English abstract).
Zhai, W., Sun, X., Sun, W., Su, L., He, X., Wu, Y., 2009. Geology, geochemistry, and genesis of Axi: a Paleozoic low-sulfidation type epithermal gold deposit in Xinjiang, China. Ore Geol. Rev. 36, 265–281.
Zhang, D.Q., Fen, C.Y., Li, D.X., She, H.Q., Dong, Y.J., 2003a. ^{40}Ar-^{39}Ar dating of adularia from Bitian sericite-adularia type epithermal Ag-Au deposit in Fujian Province and its geological significance. Miner. Deposits 22, 360–364 (in Chinese with English abstract).
Zhang, D.Q., She, H.Q., Li, D.X., Feng, C.Y., 2003b. The porphyry-epithermal metallogenic system in the Zijinshan. Acta Geol. Sinica 77, 253–261 (in Chinese with English abstract).
Zhang, D.Q., She, H.Q., Yan, S.H., Xu, W.Y., 2001. Geochemistry of Mesozoic magmatites in the Zijinshan region and implication on regional tectonic inversion. Geol. Rev. 47, 608–616 (in Chinese with English abstract).
Zhang, J.Z., 2013. Geology, exploration model and practice of Zijinshan ore concentrated area. Miner. Deposits 32, 757–766 (in Chinese with English abstract).
Zhang, L.G., 1985. The Application of the Stable Isotope to Geology. Shaanxi Science and Technology Publishing House, Xi'an, p. 267 (in Chinese with English abstract).
Zhao, X.L., Mao, J.R., Chen, R., Xu, N.Z., 2008. SHRIMP zircon dating of the Zijinshan pluton in southwestern Fujian and its implications. Geol. China 35, 590–597 (in Chinese with English abstract).
Zhong, J., Chen, Y.J., Pirajno, F., 2017a. Geology, geochemistry and tectonic settings of the molybdenum deposits in South China: a review. Ore Geol. Rev. (81), 829–855.
Zhong, J., Pirajno, F., Chen, Y.J., 2017b. Epithermal deposits in South China: geology, geochemistry, geochronology and tectonic setting. Gondwana Res. 42, 193–219.
Zhong, J., Chen, Y.J., Pirajno, F., Chen, J., Li, J., Qi, J.P., Li, N., 2014. Geology, geochronology, fluid inclusion and H-O isotope geochemistry of the Luoboling porphyry Cu-Mo deposit, Zijinshan orefield, Fujian Province, China. Ore Geol. Rev. 57, 61–77.
Zijin Mining Group Co., 2008. Reserve Verification Report in the East Section of the Yueyang Ag-Au-Cu Deposit (from August, 2002 to December, 2007) Unpublished Report (in Chinese).